Surface Heterogeneity Effects on Regional-Scale Fluxes in Stable Boundary Layers: Surface Temperature Transitions

ROB STOLL AND FERNANDO PORTÉ-AGEL

St. Anthony Falls Laboratory, Department of Civil Engineering, University of Minnesota, Minneapolis, Minnesota

(Manuscript received 1 November 2007, in final form 15 May 2008)

ABSTRACT

Large-eddy simulation, with recently developed dynamic subgrid-scale models, is used to study the effect of heterogeneous surface temperature distributions on regional-scale turbulent fluxes in the stable boundary layer (SBL). Simulations are performed of a continuously turbulent SBL with surface heterogeneity added in the form of streamwise transitions in surface temperature. Temperature differences between patches of 6 and 3 K are explored with patch length scales ranging from one-half to twice the equivalent homogeneous boundary layer height. The surface temperature heterogeneity has important effects on the mean wind speed and potential temperature profiles as well as on the surface heat flux distribution. Increasing the difference between the patch temperatures results in decreased magnitude of the average surface heat flux, with a corresponding increase in the mean potential temperature in the boundary layer. The simulation results are also used to test existing models for average surface fluxes over heterogeneous terrain. The tested models fail to fully represent the average turbulent heat flux, with models that break the domain into homogeneous subareas grossly underestimating the heat flux magnitude over patches with relatively colder surface temperatures. Motivated by these results, a new parameterization based on local similarity theory is proposed. The new formulation is found to correct the bias over the cold patches, resulting in improved average surface heat flux calculations.

1. Introduction

Surface boundary conditions in numerical models of weather and climate require the specification of the surface fluxes of heat and momentum as functions of the grid-averaged wind speed and potential temperature. These surface flux parameterizations must account for all of the dynamic interaction between the land surface and the atmosphere. Simulations have proven to be sensitive to the details of how this interaction is modeled across a wide range of scales (e.g., Viterbo et al. 1999; King et al. 2001; Lüpkes and Birnbaum 2005; Tjernström et al. 2005; King et al. 2007). This is especially true under stable atmospheric conditions (Holtslag 2006) and has led to numerous research efforts, focused on homogeneous quasi-steady stable boundary layers (e.g., Delage 1997; Mahrt 1998; Derbyshire 1999; Saiki et al. 2000; Cassano and Parish 2001; Mahrt and Vickers 2002; Cuxart et al. 2006; Beare et al. 2006).

These studies and others have contributed to the overall understanding of homogeneous stable boundary layers (SBLs). However, in general the atmospheric boundary layer (ABL) is characterized by a wide range of length and time scales that are highly dependent on the spatial distribution of land surface properties (e.g., aerodynamic roughness, land surface temperature, and soil moisture). The nonlinear relationship between land surface properties and atmospheric fluxes limits the applicability of parameterizations developed for the homogeneous ABL. Under stable conditions, local changes in atmospheric stability can further complicate modeling efforts (Mahrt 1987).

Improving models for surface heterogeneity in the ABL requires detailed spatial information about turbulent fluxes. Obtaining this information through direct measurements in the ABL is difficult and must be estimated from flux tower measurements (e.g., Chehbouni et al. 2000; Acevedo and Fitzjarrald 2001, 2003; Mahrt and

Corresponding author address: Fernando Porté-Agel, St. Anthony Falls Laboratory, 2 Third Ave. SE, Minneapolis, MN 55414.
E-mail: fporte@umn.edu

DOI: 10.1175/2008JAS2668.1

© 2009 American Meteorological Society

Unauthenticated | Downloaded 11/08/25 05:53 PM UTC

Vickers 2005), tethered-balloon systems (e.g., Derbyshire 1995; Acevedo and Fitzjarrald 2003) or aircraft flyovers (e.g., Mahrt et al. 1994, 2004). Numerical studies offer a practical alternative, and several researchers have used this approach to examine the impact of surface heterogeneity on surface flux parameterizations in neutral and convective boundary layers (e.g., Mason 1988; Claussen 1990; Avissar and Schmidt 1998; Roy and Avissar 2000; Bou-Zeid et al. 2004; Patton et al. 2005). In the SBL, the majority of studies of surface heterogeneity effects have either focused on the structure of stable internal boundary layers (e.g., Smedman et al. 1997; Mahrt et al. 2004; Skyllingstad et al. 2005, 2007) or used numerical mesoscale simulations to look at surface heterogeneity in the SBL at scales on the order of 100 km (Mahrt 1987; McCabe and Brown 2007). In a related study, Acevedo and Fitzjarrald (2001) used the large-eddy simulation technique to examine the significance of heterogeneous topography on the transition to stable conditions. They found that during the later part of the transition, advection effects control the spatial distribution of scalars and that spatial variability at scales smaller than typical mesoscale grids have important implications for nighttime forecasts. In addition, comprehensive flux aggregation studies have used Reynolds-averaged Navier–Stokes models to look at weakly stable ABLs (Claussen 1991; Wood and Mason 1991; Blyth 1995; Vihma 1995). Nonetheless, the topic of flux aggregation in the SBL at scales used in mesoscale research models (on the order of 1–10 km) has not been directly addressed without the use of highly parameterized turbulence models.

In this study, we focus on the impact of small-scale surface temperature heterogeneity on the parameterization of the average surface flux and stress in the stable atmospheric boundary layer. A series of large-eddy simulations (LES) of the SBL are performed over patches consisting of abrupt changes in surface temperature with patch sizes ranging from 100 to 400 m. The simulation results are used to evaluate three prevalent parameterization methods used in large-scale atmospheric models to calculate the average surface flux and stress over heterogeneous terrain. The paper is organized as follows: First, the three models are reviewed in section 2. Next, in section 3, the LES methodology, numerics, and subgrid-scale (SGS) models are reviewed, followed by an overview of the setup for the heterogeneous cases. Then the mean velocity and flux profiles for all of the cases are presented in section 4a. These simulation results are used in section 4b to test the performance of the models reviewed in section 2. The insight gained from these tests is then combined with theoretical arguments to develop a new model for the SBL over heterogeneous surface conditions in section 4c. Last, a summary of the research results is given in section 5.

2. Modeling average surface stresses and fluxes

Most parameterizations of ABL surface fluxes invoke Monin–Obukhov similarity theory in some way. The simplest methods calculate the average surface stress $\langle \tau_s \rangle$ and surface heat flux $\langle q_s \rangle$ directly from the grid-averaged surface properties and the grid-averaged wind speed and potential temperature. This is typically referred to as bulk similarity (Mahrt 1996; Brutsaert 1998):

$$\langle \tau_s \rangle = -C_m \langle M(Z_m) \rangle^2 \quad \text{and} \tag{1}$$

$$\langle q_s \rangle = -C_h \langle M(Z_m) \rangle \, [\langle \theta(Z_m) \rangle - \langle \theta_s \rangle] \, , \tag{2}$$

where $M = \sqrt{u^2 + v^2}$ is the wind speed, u and v are the streamwise and spanwise wind components, θ is the potential temperature, Z_m is a reference height equal to the first computation model level height, $\langle \, \rangle$ represent a spatial average over the large-scale model grid cell, and the subscript s denotes a surface value. The transfer coefficients C_m and C_h are defined using the stability corrected log-law:

$$C_m = \frac{\kappa^2}{[\ln(Z_m/z_o) - \Psi_m(Z_m/L)]^2} \quad \text{and} \tag{3}$$

$$C_h = \frac{\kappa^2}{[\ln(Z_m/z_o) - \Psi_m(Z_m/L)] \, [\alpha \ln(Z_m/z_t) - \Psi_h(Z_m/L)],} \tag{4}$$

where κ is the von Kármán constant (=0.4); z_o and z_t are the aerodynamic roughness lengths for momentum and heat, respectively, defined over the entire grid; α is an empirical constant with a value ≈0.74–1.0 (Högström 1996); Ψ_m and Ψ_h are the stability corrections for momentum and heat, respectively; and L is the Obukhov length defined by

$$L = \frac{-u_*^3 \theta_0}{\kappa g \langle q_s \rangle}, \tag{5}$$

where $u_* = \sqrt{-\langle \tau_s \rangle}$ is the surface friction velocity, θ_0 is a reference potential temperature, and g is gravitational acceleration.

Unauthenticated | Downloaded 11/08/25 05:53 PM UTC

Under stable conditions, when the heat flux is into the ground, the stability corrections for momentum and heat (Ψ_m and Ψ_h) are typically taken as linear functions of the stability parameter Z_m/L (Webb 1970; Businger et al. 1971; Kondo et al. 1978):

$$\Psi_m = -\beta_m \frac{Z_m}{L} \quad \text{and} \tag{6}$$

$$\Psi_h = -\beta_h \frac{Z_m}{L}. \tag{7}$$

The coefficients in Eqs. (6) and (7) have been given various values in the literature, with $\beta_m \approx 4.7$–7.0 and $\beta_h \approx 4.7$–7.8 (Webb 1970; Businger et al. 1971; Kondo et al. 1978; Beare et al. 2006).

Nonlinear stability corrections for the stable surface layer have also been developed. One such formulation, introduced by Beljaars and Holtslag (1991), was formulated with the intent of extending the range of applicability of surface layer similarity to larger Z_m/L values while retaining consistency with the concept of a critical Richardson number:

$$-\Psi_m = a\frac{Z_m}{L} + b\left(\frac{Z_m}{L} - \frac{c}{d}\right)\exp\left(-d\frac{Z_m}{L}\right) + \frac{bc}{d} \quad \text{and} \tag{8}$$

$$-\Psi_h = \left(1 + \frac{2}{3}\frac{aZ_m}{L}\right)^{3/2} + b\left(\frac{Z_m}{L} - \frac{c}{d}\right)\exp\left(-d\frac{Z_m}{L}\right) + \frac{bc}{d} - 1, \tag{9}$$

where the coefficients are $a = 1$, $b = 2/3$, $c = 5$, and $d = 0.35$. When Eqs. (6) and (7) or (8) and (9) are combined with Eqs. (1) and (2), the result is a pair of coupled implicit relationships for the surface stress and heat flux. To eliminate this, the stability corrections can also be defined using a bulk Richardson number in place of the stability parameter Z_m/L, following the methodology of Louis (1979).

The general bulk parameterization method is strictly only applicable to homogeneous steady flows. The accuracy of the bulk parameterization method in horizontally heterogeneous flows requires the implicit assumption that the mixing properties of turbulence will integrate any variability introduced by the surface heterogeneity. Under the full range of atmospheric stabilities and a variety of different surface property distributions, this assumption has been found to create errors in the calculation of turbulent surface fluxes (e.g., Wieringa 1986; Mahrt 1987; Mason 1988; Avissar and Pielke 1989; Wood and Mason 1991; Beljaars and Holtslag 1991; Claussen 1991; Vihma 1995; Chehbouni et al. 2000). One method proposed to deal with this problem is to define effective parameters for the land surface properties (Wieringa 1986; Taylor 1987; Mason 1988; Wood and Mason 1991; Beljaars and Holtslag 1991; Claussen 1991; Bou-Zeid et al. 2004). For example, in the transfer coefficients defined by Eqs. (3) and (4), the effective aerodynamic roughness values $z_{o,e}$ and $z_{t,e}$ for momentum and heat transport, respectively, must be prescribed.

Effective parameters have been shown to be adequate in some cases in which surface heterogeneity is limited to changes in aerodynamic roughness (Wieringa 1986; Mason 1988; Wood and Mason 1991; Claussen 1991; Bou-Zeid et al. 2004). In the case of changes in surface temperature (or, in general, surface scalar concentration), the heat flux and vertical potential temperature gradients can exhibit complex nonlinear behavior in heterogeneous flows. Mahrt (1987) showed through the use of idealized bulk Richardson number distributions that, in fact, small neutral or unstable patches within an area that would otherwise be classified as stable can dominate because of the nonlinear relation between the surface fluxes and mean profiles. This scenario precludes calculating average surface fluxes based on global parameters (e.g., $z_{o,e}$) in the general case of scalar transport over heterogeneous surfaces (Mahrt 1987; Avissar and Pielke 1989; Claussen 1991).

To avoid these problems and those associated with the use of Monin–Obukhov similarity theory over heterogeneous terrain, the tile model was introduced (Avissar and Pielke 1989; Claussen 1991). In this approach, the wind speed and potential temperature at the reference level Z_m are used with the local surface properties and stability corrections to calculate local surface fluxes over homogeneous subareas:

$$\langle \tau_s \rangle = -\sum_i^n f_i \left[\frac{\langle M(Zm)\rangle \kappa}{\ln(Z_m/z_{o,i}) - \Psi_m(Z_m/L_i)}\right]^2 \quad \text{and} \tag{10}$$

$$\langle q_s \rangle = -\sum_i^n f_i \frac{\kappa^2 \langle M(Z_m)\rangle \, [\langle \theta(Z_m)\rangle - \theta_{s,i}]}{[\ln(Z_m/z_{o,i}) - \Psi_m(Z_m/L_i)]\,[\alpha \ln(Z_m/z_{t,i}) - \Psi_h(Z_m/L_i)]}, \tag{11}$$

where n is the total number of homogeneous subareas or tiles, f_i is the fractional coverage of each subarea, $z_{o,i}$ and $z_{t,i}$ are the aerodynamic roughness values defined over each subarea, $\theta_{s,i}$ is the subarea surface temperature, and L_i is the Obukhov length defined with each individual subarea's surface flux values. The subareas,

Unauthenticated | Downloaded 11/08/25 05:53 PM UTC

typically referred to as tiles, are defined as regions with similar land use categories. This saves computational time over the alternative of systematically breaking up the entire grid area into equally sized subareas, which is sometimes referred to as the mosaic approach (Arola 1999; Ament and Simmer 2006).

Breaking up the grid cell introduces the possibility that even in an SBL, the focus of this paper, some tiles may have surface temperature values in excess of the grid-averaged potential temperature at Z_m. When this happens, stability corrections appropriate for convective conditions are needed. Ordinarily, the stability corrections of Paulson (1970) are used with the tile model (Avissar and Pielke 1989; Arola 1999):

$$\Psi_m = 2\ln\left[\frac{1}{2}(1+x)\right] + \ln\left[\frac{1}{2}(1+x^2)\right] - 2\tan^{-1}[x] + \pi/2 \quad \text{and} \tag{12}$$

$$\Psi_h = 2\alpha \ln\left[\frac{1}{2}(1+y)\right], \tag{13}$$

where $x = (1 - \gamma_m Z_m/L)^{1/4}$ and $y = (1 - \gamma_h Z_m/L)^{1/2}$. The empirical constants γ_m and γ_h have been assigned different values, with $\gamma_m \approx 15$–28 and $\gamma_h \approx 9$–15 (Businger et al. 1971; Dyer and Bradley 1982; Högström 1996).

The tile method assumes that vertical fluxes over each patch are much larger than advection effects between patches. Blyth et al. (1993), Blyth (1995), Arola (1999) and Ament and Simmer (2006) recommend extending the tile model to heterogeneous flows at which this assumption fails by modifying Eqs. (10) and (11) to be applied at a vertical height scale termed the "blending height." This is the height at which the flow becomes approximately homogeneous (Wieringa 1986; Mason 1988; Wood and Mason 1991; Claussen 1990, 1991). Two different definitions for the blending height are most commonly used. Mason (1988) uses heuristic arguments and linear perturbation analysis to give the following estimate for the blending height for momentum l_b in the ABL:

$$l_b\left[\ln\left(\frac{l_b}{z_{o,e}}\right)\right]^2 = 2\kappa^2 L_c, \tag{14}$$

where L_c is the scale of horizontal variation. Wood and Mason (1991) broadened this definition to include stability effects and a separate blending height for temperature in the presence of heterogeneous surface flux distributions. The second definition for the blending height was developed by Claussen (1990, 1991) by finding the height that minimizes the error associated with the assumptions of horizontal homogeneity and equilibrium with the local surface. This height is analogous to the diffusion height scale.

The stability-corrected version of Eq. (14) gives similar estimates for l_b; therefore, in practice Eq. (14) is used for a variety of atmospheric stability conditions without differentiating between the blending height for momentum and temperature (Blyth 1995; Arola 1999; Ament and Simmer 2006). For small-scale heterogeneity ($\leq$5 km), l_b is likely to be smaller than the typical model reference height. Consequently, to properly evaluate Eqs. (10) and (11) at l_b, the mean wind speed and potential temperature must be extrapolated down from Z_m. Note that $\langle M(z)\rangle$ and $\langle\theta(z)\rangle$ are extrapolated down to l_b using Monin–Obukhov theory for the grid-averaged flow [Eqs. (1) and (2)] with the assumption that

$$\frac{\langle M(Z_m)\rangle}{\langle M(l_b)\rangle} = \frac{\ln(Z_m/z_{o,e}) - \Psi_m(Z_m/L_{\text{eff}})}{\ln(l_b/z_{o,e}) - \Psi_m(l_b/L_{\text{eff}})} \quad \text{and} \tag{15}$$

$$\frac{\langle\theta(Z_m)\rangle}{\langle\theta(l_b)\rangle} = \frac{\alpha\ln(Z_m/z_{t,e}) - \Psi_h(Z_m/L_{\text{eff}})}{\alpha\ln(l_b/z_{t,e}) - \Psi_h(l_b/L_{\text{eff}})}, \tag{16}$$

where L_{eff} is an effective Obukhov length for the mean flow field, usually simply defined as $L_{\text{eff}} = L$ (Wood and Mason 1991; Blyth et al. 1993; Arola 1999). The average surface stress and flux are then calculated by evaluating Eqs. (10) and (11) at l_b, using the estimates for $\langle M(l_b)\rangle$ and $\langle\theta(l_b)\rangle$ from Eqs. (15) and (16).

3. Numerical simulations

In this section we give a brief overview of the numerical code used in this study. It was developed by Porté-Agel et al. (2000) and Porté-Agel (2004) and then modified for use in heterogeneous flows by Stoll and Porté-Agel (2006a). The code solves the incompressible filtered continuity, and conservation of momentum and heat equations. Application of a filter to these equations results in two unknown quantities that must be parameterized, the SGS stress and the SGS flux. They are modeled with recently developed scale-dependent Lagrangian dynamic models (Stoll and Porté-Agel 2006a). These models have the ability to dynamically adjust to the local turbulence field and have been successfully applied to neutral homogeneous and heterogeneous ABLs (Stoll and Porté-Agel 2006a) and to the homogeneous SBL (Stoll and Porté-Agel 2008). The base models are eddy-viscosity and eddy-diffusivity models for the SGS stress and flux, respectively. The eddy viscosity is modeled using a mixing length approximation (Smagorinsky 1963), and the Smagorinsky coefficient (C_S) and the lumped coefficient ($C_S^2 \text{Pr}_{\text{sgs}}^{-1}$), which comprises the CS and the SGS Prandtl number, are both independently computed dynamically at every position in the flow as the flow evolves in time following fluid particle trajectories (Stoll and Porté-Agel 2006a).

Unauthenticated | Downloaded 11/08/25 05:53 PM UTC

Horizontal derivatives are discretized using spectral methods and the vertical derivatives with second-order central differences. Time advancement is accomplished using an explicit second-order Adams–Bashforth method. Lateral boundary conditions are assumed to be periodic, and the top boundary condition is zero stress/flux with Rayleigh dampening in the top 100 m of the domain, following Beare et al. (2006).

The surface boundary conditions are specified through the local application of Monin–Obukhov similarity theory. Although Monin–Obukhov theory was developed for homogeneous steady flows, in LES of the ABL it is commonly applied locally to relate the resolved wind speed and potential temperature to the filtered surface stress and heat flux (Moeng 1984; Mason and Callen 1986; Bou-Zeid et al. 2004; Patton et al. 2005; Stoll and Porté-Agel 2006b). The specific application used here follows closely with that used by Stoll and Porté-Agel (2008). At surface grid points where the local surface flux is negative, Eqs. (6) and (7) are applied at the first computational level in the vertical direction, with an Obukhov length defined by the local (instantaneous) surface fluxes. At surface grid points where the advection of cold air over regions with a relatively warmer surface temperature results in locally unstable conditions, Paulson's (1970) stability corrections [Eqs. (12) and (13)] are used with a local Obukhov length and parameters $\gamma_m = \gamma_h = 15$.

To study how surface temperature heterogeneity affects ABL dynamics under stable stratification, a set of simulations is performed over different surface temperature distributions. Because the stable boundary layer is characterized by small fluxes, intermittency, and the presence of nonturbulent physics (e.g., gravity waves and radiative flux divergence), it is difficult to study experimentally or numerically (e.g., Mahrt 1998; Saiki et al. 2000). To limit these other factors and focus on turbulent transport processes associated with heterogeneous surface conditions, a well-established, idealized, and relatively simple SBL case is needed. The Global Energy and Water Cycle Experiment (GEWEX) Atmospheric Boundary Layer Study (GABLS) meets this criterion (Beare et al. 2006). Other than the addition of heterogeneous surface temperature distributions, the only notable change to the basic GABLS simulation parameters is the horizontal domain size. It has been increased from 400 to 800 m. This horizontal domain size was also used by Beare and MacVean (2004) and Stoll and Porté-Agel (2008) when examining the homogeneous SBL. The increased length of the domain facilitates the study of a larger range of surface heterogeneity scales. The base simulation parameters are summarized in Table 1.

TABLE 1. Base parameters for the homogeneous and heterogeneous SBL simulations. The subscripts *x*, *y*, and *z* refer to the streamwise, spanwise, and surface-normal directions, respectively.

Description	Symbol	Value
Geostrophic wind	U_g	8 m s^{-1}
Aerodynamic roughness	z_o	0.1 m
Coriolis parameter	f_c	1.39×10^{-4} s^{-1}
Domain dimensions	L_x, L_y, L_z	800, 800, 400 m
Number of grid points	N_x, N_y, N_z	128, 128, 128
Grid spacing	Δ_x, Δ_y, Δ_z	6.25, 6.25, 3.15 m
Initial velocity	u, v, w	8, 0, 0 m s^{-1}
Initial θ ($z < 100$ m)	Θ	265 K
Initial lapse rate ($z > 100$ m)	Γ_l	0.01 K m^{-1}

The surface heterogeneity consists of abrupt transitions in surface temperature in the streamwise direction. This forms a series of spanwise homogeneous surface temperature patches that alternate between two temperature values whose mean is equal to the surface temperature used in the GABLS study (initially 265 K). A total of eight simulations were performed: one homogeneous case, three cases with a temperature jump between patches of 3 K, three with a temperature jump between patches of 6 K, and one high-resolution heterogeneous case. The temperature jumps are created by specifying different cooling rates for each patch while keeping the average cooling rate over the entire domain surface equal to that used in the GABLS study (0.25 K hr^{-1}). After 8 h, the cooling rate was returned to its average value and the simulations were continued for an additional 4 h. This is required to ensure that the simulations reach a quasi-steady state. The patch cooling rates were chosen to create the desired temperature differences after 8 h of simulation. For the 3-K temperature jump, this corresponds to patches with cooling rates alternating between 0.4375 K hr^{-1} for the colder patch and 0.0625 K hr^{-1} for the warmer patch. For the 6-K temperature jump simulations, the patches alternate between a cooling rate of 0.625 K hr^{-1} and a small heating rate of 0.125 K hr^{-1}. It is important to note that with these cooling (and heating for the 6-K temperature jump cases) rates, all of the simulations resulted in negative (into the ground) average surface heat fluxes throughout the simulations. The surface temperature time evolution for the two different cases (3 and 6 K) is depicted in Fig. 1 along with examples of the time evolution for the domain-average surface heat flux and shear stress. Each temperature jump was tested with three different patch lengths: 100, 200, and 400 m. These lengths correspond to approximately 2 (400 m), 1 (200 m), and 0.5 (100 m) times the boundary layer height calculated at the end of the homogeneous run. In addition to the base LES grid resolution of $6.25 \times 6.25 \times 3.15$ m^3

Unauthenticated | Downloaded 11/08/25 05:53 PM UTC

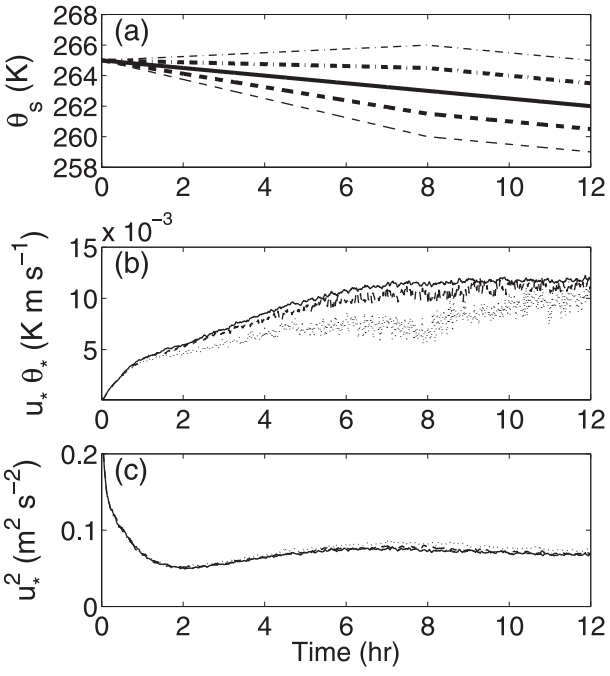

FIG. 1. Time evolution of the surface temperature used in the simulations and the resulting average surface heat flux and shear stress from representative cases. (a) Surface temperature evolution where the lines correspond to a 3-K cold patch (thick dashed), 3-K warm patch (thick dashed–dotted), 6-K cold patch (thin dashed), 6-K warm patch (thin dashed–dotted), and the average case (thick continuous). (b) Surface heat flux evolution from the 3-K, 400-m (dashed) and 6-K 400-m (dotted) patch cases and the homogeneous case (continuous). (c) Surface shear stress evolution from the 3-K 400-m (dashed) and 6-K 400-m (dotted) patch cases and the homogeneous case (continuous).

(in the streamwise, spanwise, and surface-normal directions, respectively), a high-resolution simulation of the 6-K temperature jump, 400-m patch size case was performed with a grid resolution of $4.17 \times 4.17 \times 2.09$ m^3. This simulation was used to examine how the representation of the surface temperature transitions is affected by changes in grid resolution. Because the lateral boundary conditions are periodic, the patches infinitely repeat in the streamwise direction.

4. Results

a. Average statistics

In this section we begin to explore how heterogeneity affects the SBL using the suite of simulations described in section 3. Two-dimensional spanwise-averaged and one-dimensional horizontal plane–averaged values of first- and second-order boundary layer statistics are presented. Fluctuations needed to calculate turbulent fluxes in the boundary layer are defined as deviations from the horizontally averaged quantities so that $\xi' = \xi - \langle\xi\rangle$, where ξ is the variable of interest (i.e., a velocity component or the potential temperature). The heterogeneous cases are examined for the signature of the heterogeneity and compared with the base homogeneous case studied in detail by Stoll and Porté-Agel (2008). Results are averaged over the last 1 h of simulation time (hours 11–12). The bulk characteristics for the heterogeneous simulations and the homogeneous base case—including the boundary layer height H, average friction velocity u_*, surface temperature scale $\theta_* = -\langle q_s\rangle u_*^{-1}$, and Obukhov length L—are given in Table 2. The boundary layer height H is defined as (1.0/0.95) times the height where the mean stress goes to 5% of its surface value following Kosović and Curry (2000).

TABLE 2. Mean boundary layer characteristics for the different surface types characterized by the jump (in K) and the patch length (in m): homogeneous case (Hom); 3 K, 400 m (Het3–400); 3 K, 200 m (Het3–200); 3 K, 100 m (Het3–100); 6 K, 400 m (Het6–400); 6 K, 200 m (Het6–200); 6 K, 100 m (Het6–100). The high-resolution case is denoted by 192^3. The symbols correspond to those used in the figures throughout the paper.

Case	Symbol	H (m)	u_* (m s^{-1})	θ_* (K)	L (m)
Hom	+	175	0.260	0.0451	101
Het3–400	○	181	0.263	0.0426	109
Het3–200	△	179	0.263	0.0423	110
Het3–100	◇	180	0.263	0.0420	111
Het6–400	▽	196	0.271	0.0363	136
Het6–200	□	197	0.272	0.0357	139
Het6–100	◁	199	0.274	0.0353	143
Het6–400 192^3	▷	190	0.265	0.0348	135

1) TWO-DIMENSIONAL BOUNDARY LAYER STRUCTURE

The surface temperature heterogeneity modifies the distribution of the surface fluxes of heat and momentum. Local advection of relatively cold air from the colder patches over the warmer surface temperature patches results in positive surface heat fluxes over these patches. Conversely, local advection of warm air over the colder surface patches gives rise to negative surface heat fluxes. The changes in local stability created by these surface heat flux transitions result in an adjustment of the local surface shear stress over each patch. Over the colder (stable) patches the effect of stratification acts to reduce the shear stress, and over the hotter (unstable) patches the shear stress is enhanced by convective production of turbulence. This scenario is illustrated in Fig. 2 using the Het6 simulations. (See Table 2 for case names and descriptions.) The spanwise-averaged surface heat fluxes (q_s) and shear stresses (τ_s),

Unauthenticated | Downloaded 11/08/25 05:53 PM UTC

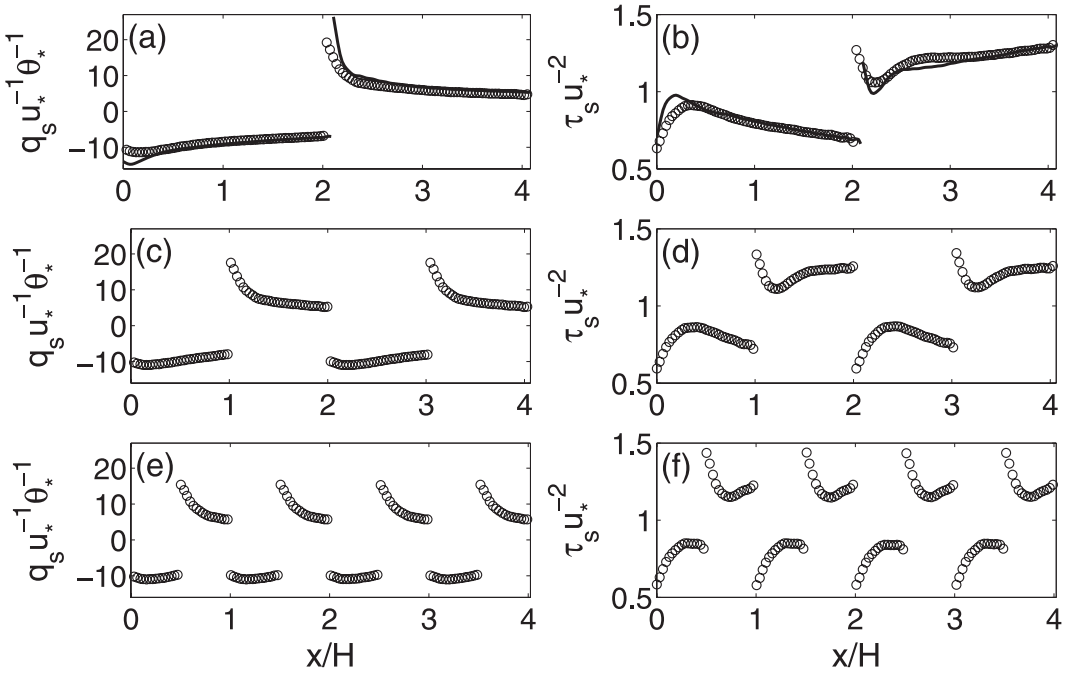

FIG. 2. Normalized spanwise-averaged surface flux distributions from simulations over streamwise transitions in surface temperature: (a) $q_s u_*^{-1}\theta_*^{-1}$ from the Het6–400 (circles) and Het6–400 192^3 (lines) cases; (b) $\tau_s u_*^{-2}$ from the Het6–400 (circles) and Het6–400 192^3 (lines) cases; (c) $q_s u_*^{-1}\theta_*^{-1} w$ from the Het6–200 case; (d) $\tau_s u_*^{-2}$ from the Het6–200 case; (e) $q_s u_*^{-1}\theta_*^{-1}$ from the Het6–100 case; (f) $\tau_s u_*^{-2}$ from the Het6–100 case.

normalized with the average boundary layer parameters presented in Table 2, are plotted versus the nondimensional streamwise distance xH^{-1}. Immediately after the cold-to-hot transitions the surface heat flux reaches a maximum positive value. For the hot-to-cold transitions, the maximum negative surface heat flux also occurs after the transition, but instead of a sharp decline it gradually decreases in magnitude throughout the length of the patch. None of the surface fluxes reach full equilibrium (defined as a constant value in the streamwise direction) over any of the patches, regardless of the type of transition (hot-to-cold or cold-to-hot) or the patch length. This is most likely attributable to the observed slow adjustment of the SBL to changes in surface conditions (Derbyshire 1995). In Figs. 2a,b, the high-resolution Het6–400 case surface heat flux and shear stress, respectively, are given alongside of the base resolution results. For the heat flux and the shear stress, the general trends in the near-transition region and the strength of the heat flux and shear stress jumps away from the transitions are nearly identical between the base and high-resolution cases. The main effect of increasing the resolution is apparently to sharpen the details in the transition regions. The only discrepancy is the slight shift toward larger xH^{-1} values for the transition point. This is attributed to the different values of H for the two simulations (see Table 2). These effects of increasing the simulation resolution are indicative of the effects seen in subsequent plots throughout this section. Profiles in regions with large gradients are refined, but general trends remain consistent after allowing for changes in H. The Het3 cases have similar patterns in the surface heat flux and shear stress distributions. The main difference is that the deviations from the mean heat flux and shear stress are smaller in magnitude for the Het3 cases.

The surface flux distributions are directly linked to the structure of the thermal boundary layer. The transitions from hot to cold or cold to hot surface temperature result in the formation of thermal internal boundary layers (IBLs). These IBLs grow vertically over each patch in the flow direction up to the height at which the flow homogenizes (Brutsaert 1998; Mahrt 2000). In Fig. 3 the thermal IBL structure from the Het6 cases is depicted by plotting the spanwise-averaged vertical gradients of the potential temperature normalized by the height and the average surface temperature scale from Table 2. Two distinct regions are clear in the graphs: one over the cold patches, where the surface heat flux is negative and the gradients are greater than zero, which indicates an increasing potential temperature with height; and another over the hotter patches

Unauthenticated | Downloaded 11/08/25 05:53 PM UTC

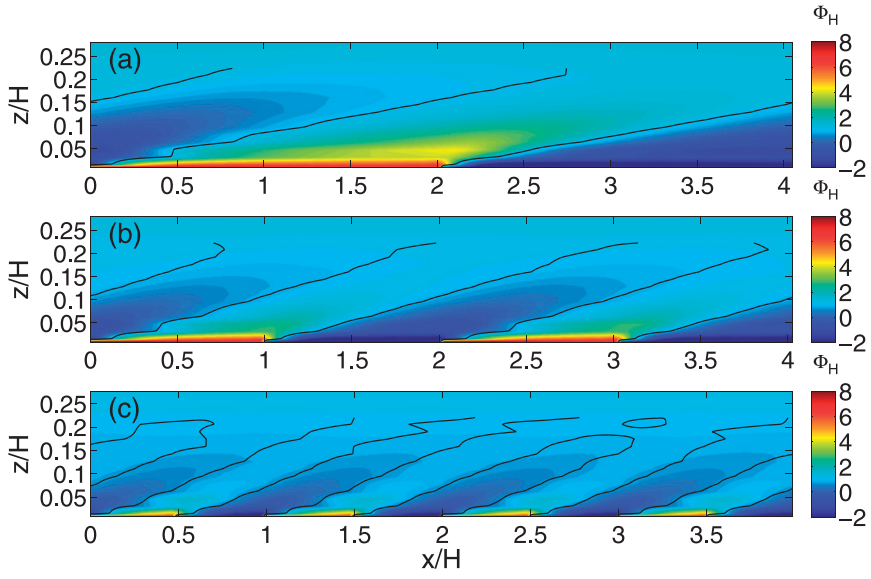

FIG. 3. Nondimensional spanwise- and time-averaged potential temperature vertical gradients $\Phi_H = \kappa z \theta_*^{-1} \partial\theta/\partial z$ for cases (a) Het6–400, (b) Het6–200, and (c) Het6–100. The black contours trace the points where the spanwise-averaged Φ_H values are equal to the horizontal plane–averaged ones at a given height. These points can be used as a measure of the internal boundary layer height and indicate where the potential temperature field is in equilibrium with the surface (Bou-Zeid et al. 2004; Stoll and Porté-Agel 2006a).

where the gradients are less than zero, characteristic of an unstable boundary layer. The two regions are separated by local temperature inversions (indicated by the black contours). The IBL growth in the Het3 simulations follows similar patterns. The nondimensional spanwise-averaged gradients have the same spatial distribution but with a smaller range of values.

Within the different IBL regions, the heat and momentum flux profiles adjust to the surface fluxes in a consistent manner. For the heat flux, this is illustrated in Fig. 4 with the Het6–400 case. Over the cold patches (Fig. 4a), the flow of warm air over the colder surface results in a maximum negative heat flux at the surface (depicted in Fig. 2a) immediately after the transition. In this region, where the thermal IBL is shallow, the magnitude of the vertical heat flux decreases rapidly with height, quickly becoming positive and reflecting the upwind convective boundary layer heat flux profile. Away from the transition in the streamwise (x) direction, as the surface heat flux decreases in magnitude and the thermal IBL grows, the heat flux in the boundary layer at a given nondimensional height zH^{-1} decreases and the heat flux profile in the IBL becomes nearly linear. Over the hot patch (Fig. 4b) the opposite happens: The upwind heat flux profile from the cold patch erodes, with what begins as a thin region of positive flux growing until the entire surface layer is consumed.

The local height-dependent friction velocity $[= (-\tau)^{1/2}]$ normalized by u_* is plotted at different streamwise positions in Fig. 5. Over the cold patch, just after the transition the local friction velocity increases with height until it reaches the upwind profile. Away from the transition, an equilibrium zone forms where the local friction velocity decreases with height. Above this zone, the local friction velocity again increases until it reaches the upwind profile. For the cold-to-hot transition, the local friction velocity does not have the same clear change from increasing to decreasing with height; instead, it decreases with height throughout most of the thermal IBL. Overall, the local friction velocity deviations from the mean are much smaller (<25%) than that of the heat flux in Fig. 4.

2) VERTICAL PROFILES

The average wind speed and potential temperature at the lowest computational level are usually the only boundary layer variables available for surface flux parameterizations in large-scale weather and climate models. In Fig. 6 the mean profiles of each of these variables are presented for all the simulations. The wind speed profiles (Fig. 6a) from all the cases exhibit an elevated wind maximum near their respective boundary layer tops. The existence of this nocturnal jet agrees with Nieuwstadt's theoretical model (Nieuwstadt 1984,

Unauthenticated | Downloaded 11/08/25 05:53 PM UTC

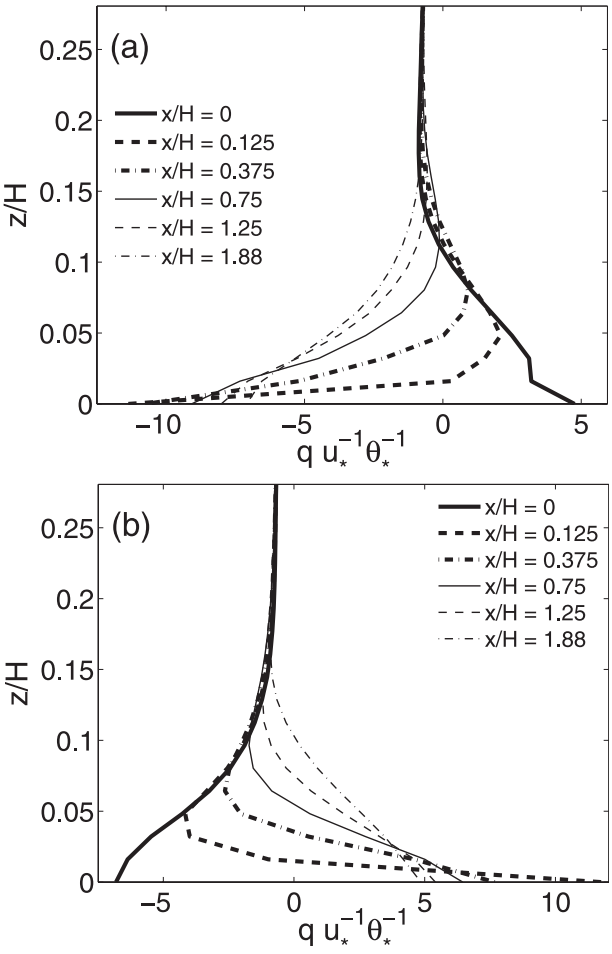

FIG. 4. Profiles of the spanwise- and time-averaged height-dependent vertical heat flux at selected streamwise positions from the case Het6–400 over the (a) cold and (b) hot surface temperature patches. The streamwise positions xH^{-1} in the legends are referenced to the transition points immediately upwind of each patch.

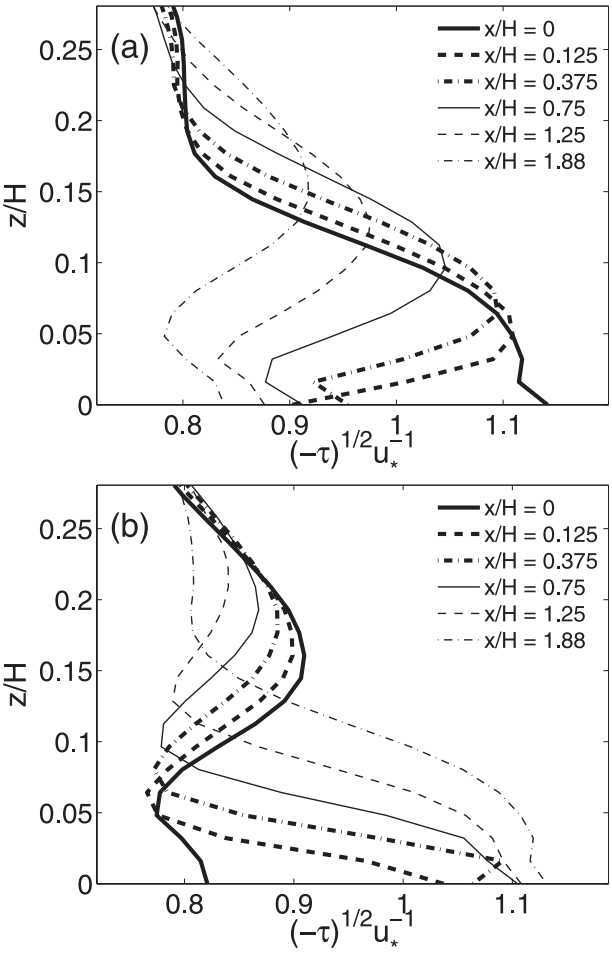

FIG. 5. As in Fig. 4, but for the spanwise- and time-averaged height-dependent friction velocity.

1985) for the homogeneous steady-state SBL. The maximum speed value within the jet is unaffected by the different patch sizes or surface temperature contrasts, but the location of the wind maximum shifts for the two different temperature jumps. The larger the jump, the higher up the nocturnal jet occurs. In general, the patch size appears to have very little effect on the wind speed profiles. The larger effect of the temperature jump, compared with the patch size, is consistent with the changes in boundary layer height (H) and friction velocity (u_*) shown in Table 2. Normalization of the ordinate in Fig. 6a by H (not shown) demonstrates that the change in the location of the nocturnal jet is mostly a manifestation of the increased boundary layer height. In the lowest 50 m of the domain all the wind profiles have minimal deviations from the homogeneous case.

All of the mean potential temperature profiles in Fig. 6b have positive curvature above the surface inversion, as implied by Nieuwstadt's model (Nieuwstadt 1984, 1985). These profiles show a similar systematic dependence on surface heterogeneity as the mean wind speed profiles. The Het3 and Het6 simulations all have an increased potential temperature throughout the boundary layer with respect to the homogeneous case. This pattern agrees with the decreased average surface flux and increased Obukhov lengths. Compared to changing the patch temperature contrast, the potential temperature profiles do not show significant dependence on the patch length scale for the range of patch length scales tested here.

Most surface flux models rely on Monin–Obukhov similarity theory to relate surface fluxes to the average wind speed and potential temperature at the first computational level (Beljaars and Holtslag 1991; Delage 1997; Brutsaert 1998; King et al. 2001). The central tenet

Unauthenticated | Downloaded 11/08/25 05:53 PM UTC

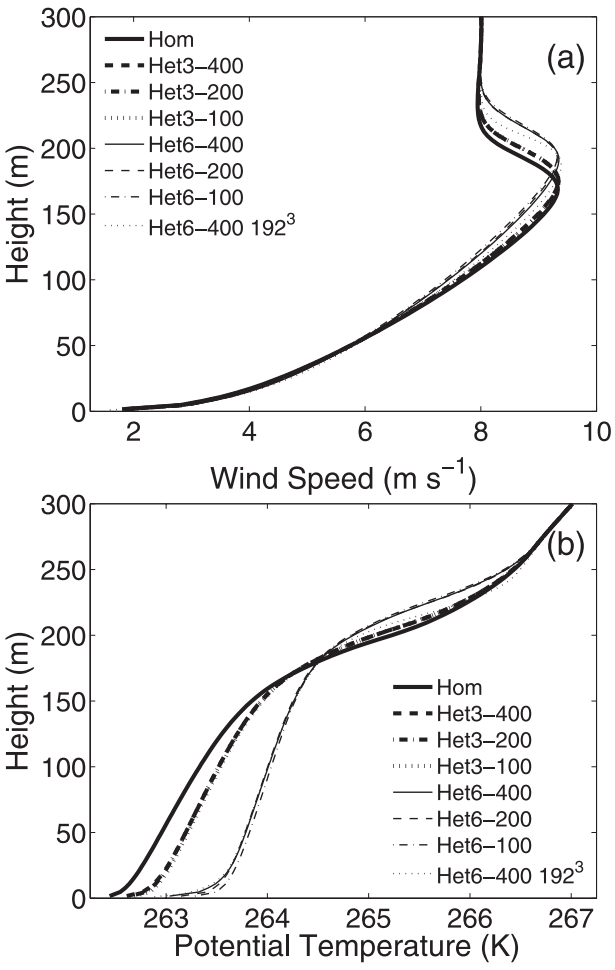

FIG. 6. (a) Mean wind speed and (b) potential temperature profiles averaged over the last 1 h of the simulation for homogeneous and heterogeneous SBL simulations. Legend abbreviations are as in Table 2.

of this type of similarity theory is that within the surface layer, nondimensional turbulence statistics depend only on the stability parameter zL^{-1}. For the nondimensional shear and potential temperature gradients this is expressed as

$$\left(\frac{\kappa z}{u_*}\right)\frac{\partial\langle M\rangle}{\partial z}=\Phi_M\left(\frac{z}{L}\right) \quad \text{and} \tag{17}$$

$$\left(\frac{\kappa z}{\theta_*}\right)\frac{\partial\langle\theta\rangle}{\partial z}=\Phi_H\left(\frac{z}{L}\right). \tag{18}$$

Often these gradients are parameterized as linear functions of zL^{-1} in the stable surface layer (Businger et al. 1971):

$$\Phi_M=1+\beta_m\frac{z}{L}, \tag{19}$$

$$\Phi_H=\alpha+\beta_h\frac{z}{L}, \tag{20}$$

where the constants α, β_m, and β_h are the same as in Eqs. (4), (6), and (7), respectively. Beljaars and Holtslag (1991) found a better fit to their data using a nonlinear relation:

$$\Phi_M=1+\frac{z}{L}\left[a+be^{-d\frac{z}{L}}\left(1+c-d\frac{z}{L}\right)\right], \tag{21}$$

$$\Phi_H=1+\frac{z}{L}\left[a\left(1+\frac{2}{3}\frac{az}{L}\right)^{1/2}+be^{-d\frac{z}{L}}\left(1+c-d\frac{z}{L}\right)\right], \tag{22}$$

where the constants a, b, c, and d are the same as in Eqs. (8) and (9).

To explore the validity of Monin–Obukhov similarity theory over heterogeneous surface temperature distributions, the nondimensional gradients from the heterogeneous and homogeneous simulations are plotted as functions of zL^{-1} in Fig. 7. The gradients are compared to the empirical formulations given by Eqs. (19)–(22).

The heterogeneous surface temperature distributions have almost zero effect on the average nondimensional shear depicted in Fig. 7a. This agrees with the mean wind speed profiles in Fig. 6a in which no clear trend is observed in the near-surface region. It appears that although the heterogeneity affects the boundary layer height and surface shear stress, it does not change the functional relationship between the mean surface stress and the wind speed at the lowest levels. Therefore, Eq. (19) may be useful when modeling the average surface stress in a SBL with heterogeneous surface temperature distributions.

In contrast to Φ_M, the nondimensional potential temperature gradients presented in Fig. 7b have a clear dependence on the surface temperature distribution. The surface heterogeneity results in increased values of Φ_H near the ground with respect to the homogeneous case. The patch size plays an important role in determining the shape of the potential temperature profile at the levels closest to the ground. In general, the gradients are reduced for a given zL^{-1} value as the patch size decreases. Although the patch size is important, the difference in temperature between the two patches clearly dominates. Its effect is strong enough that both the Het6–400 and Het6–200 cases have significantly increased gradients for the majority of the near-surface region. For all the heterogeneous cases, the Φ_H values decrease or remain constant with increasing zL^{-1} up to a case-dependent zL^{-1} value. This value increases with increasing patch size and, to a lesser extent, with increasing temperature contrast between the patches. In standard SBL parameterizations, Φ_H is generally thought to increase with the

Unauthenticated | Downloaded 11/08/25 05:53 PM UTC

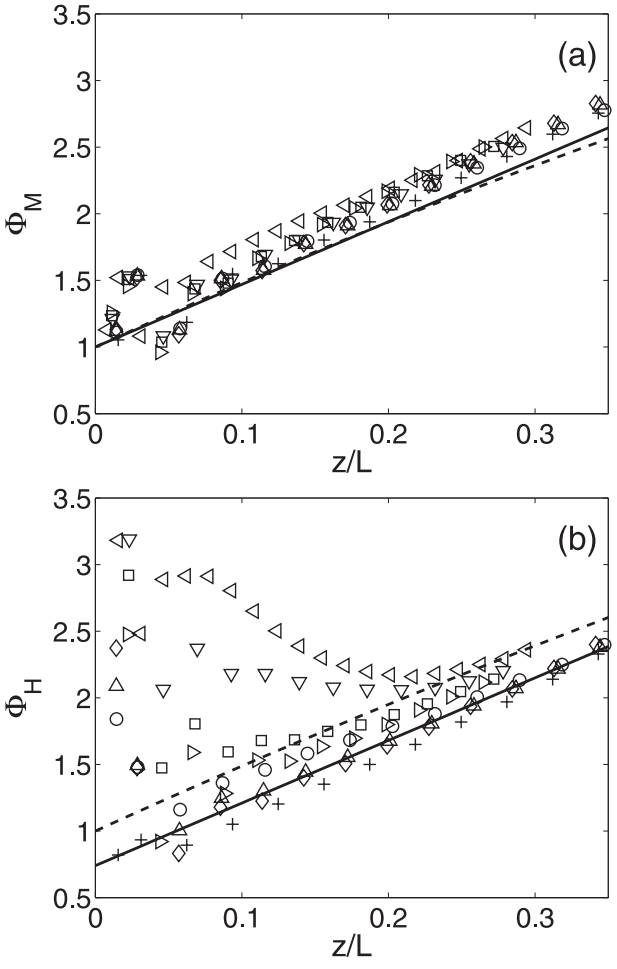

FIG. 7. Nondimensional (a) shear and (b) potential temperature gradients as functions of z/L in the lowest 40 m of the domain. Graph symbol definitions are given in Table 2; the solid and dashed lines correspond to the formulations proposed by Businger et al. (1971) and Beljaars and Holtslag (1991), respectively.

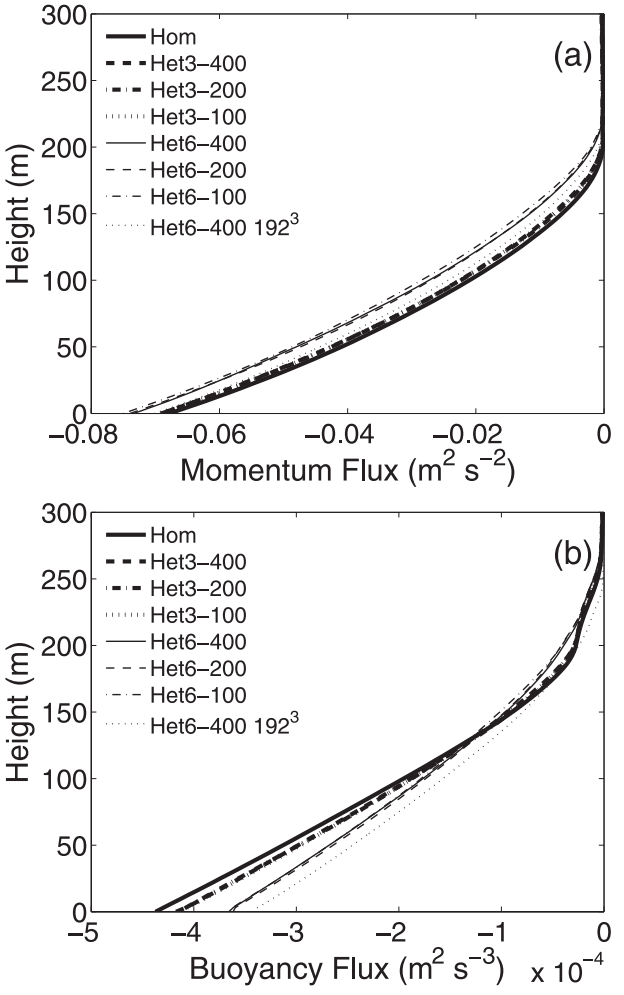

FIG. 8. Total (a) momentum and (b) buoyancy flux profiles from homogeneous and heterogeneous SBL simulations. The legend abbreviations are as in Table 2.

stability parameter zL^{-1} [e.g., Eqs. (20) and (22)], not decrease or remain constant. A similar phenomenon has been described previously. It is speculated that in a heterogeneous SBL patches that are relatively warmer (and thus produce locally unstable conditions) can dominate the area-averaged surface fluxes, resulting in a decoupling of the potential temperature gradients and the surface fluxes (Mahrt 1987; Claussen 1991; Blyth et al. 1993; Blyth 1995; Mahrt 1996; Mahrt and Vickers 2005). A similar situation exists here. Increased Φ_H values are associated with boundary layers that, on average, should be less stable. For example, in Table 2 the Het6 cases all have the largest Obukhov lengths and the smallest (in magnitude) heat fluxes. Normally, this would lead to smaller gradients, but here, because the boundary layer potential temperature is greater (see Fig. 6b) while the surface temperature stays the same, the gradients near the surface are very large. This indicates that proper estimation of the average surface heat flux for the heterogeneous cases presented here cannot be made by assuming homogeneity and using the average potential temperature profile with a typical similarity formulation [e.g., Eq. (2)]. In section 4b this will be elaborated on as part of the evaluation of methodologies designed to compute average surface fluxes over heterogeneous land surface cover.

The average total (resolved plus subgrid) momentum ($\langle u'w' \rangle$) and buoyancy ($g\theta_o^{-1}\langle w'\theta' \rangle$) flux profiles are presented in Fig. 8. The momentum flux in the boundary layer increases with increasing temperature contrast between patches. The size of the patches has a minimal effect. The increase agrees with the friction velocity and boundary layer height values in Table 2. The total buoyancy flux in Fig. 8b decreases throughout

Unauthenticated | Downloaded 11/08/25 05:53 PM UTC

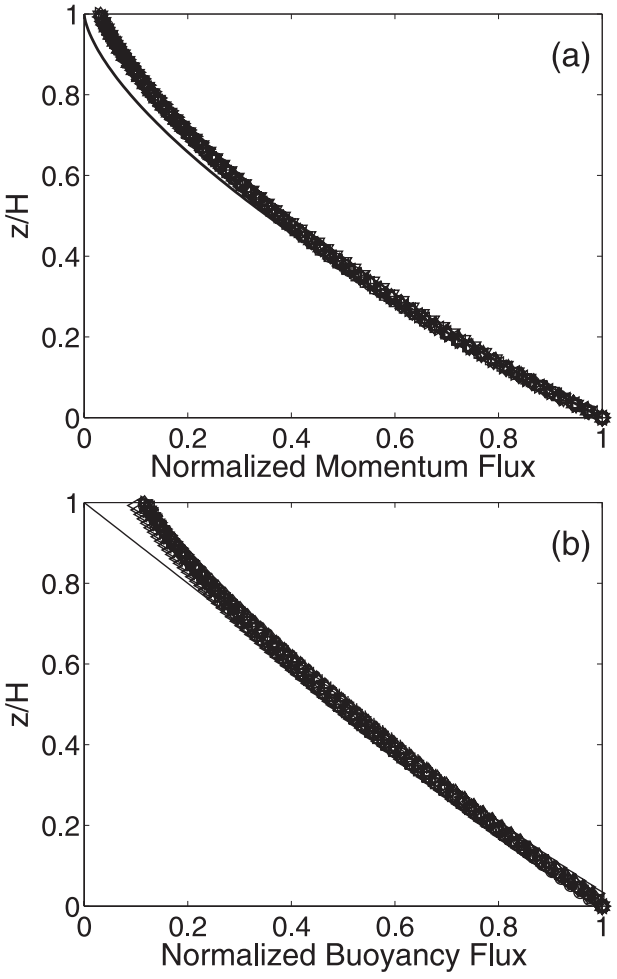

FIG. 9. (a) Total momentum flux profiles normalized by the mean surface stress and (b) total buoyancy flux profiles normalized by their surface values from heterogeneous SBL simulations plotted vs. the dimensionless height zH^{-1}. The graph symbols are defined in Table 2; the solid lines represent the predictions of Nieuwstadt (1984, 1985).

the boundary layer for larger surface temperature contrasts. This agrees with the decrease in θ_* for the heterogeneous cases compared with the homogeneous case (see Table 2). Again, the patch size has a much smaller effect.

In the steady homogeneous SBL, the momentum and buoyancy fluxes normalized by their respective surface values are expected to depend solely on the dimensionless height zH^{-1} (Nieuwstadt 1984, 1985). The normalized momentum flux should follow zH^{-1} to the 3/2 power and the buoyancy flux should be linear with zH^{-1}. To check this in the heterogeneous simulations, the normalized momentum and buoyancy fluxes are plotted in Fig. 9. All of the simulations agree with these predictions.

b. *Evaluation of existing heterogeneous surface flux models*

In the introduction, three basic methodologies for calculating the area-averaged surface stress and heat flux were introduced. These included the basic bulk parameterization (Mahrt 1996; Brutsaert 1998), the mosaic or tile method (Avissar and Pielke 1989; Claussen 1991), and the extended tile method (Blyth et al. 1993; Blyth 1995; Arola 1999). In this section, the LES 3D velocity and potential temperature fields are used to evaluate these models. Modeled fluxes are computed with each method from the LES average wind speed and potential temperature profiles and the heterogeneous surface temperature distributions. These modeled fluxes are then compared to the surface stresses and fluxes obtained from the simulations. In addition to the six heterogeneous cases, the homogeneous case, studied in detail by Stoll and Porté-Agel (2008), and the high-resolution Het6–400 case are also presented as references. The flux aggregation models are tested for a range of large-scale atmospheric model lowest computational levels from 10 to 50 m. To avoid the need to interpolate the LES average potential temperature and velocity profiles, the chosen model levels correspond to the LES vertical grid point locations. In all of the flux-aggregation models, the linear stability corrections of Businger et al. (1971) are adopted when appropriate for stable conditions (with $\beta_m = \beta_h = 4.7$ and $\alpha = 0.74$), and the stability corrections of Paulson (1970) are used when needed for unstable conditions (with $\gamma_m = \gamma_h = 15$ and $\alpha = 0.74$).

We begin by examining the bulk parameterizations for the average surface flux and stress given by Eqs. (1) and (2). This method corresponds to directly integrating the nondimensional potential temperature and velocity gradients shown in Fig. 7. The surface heat flux estimated from Eq. (2) divided by the LES surface heat flux is plotted in Fig. 10a for all the cases. For the homogeneous case, the modeled results deviate from the LES surface heat flux by approximately 5% throughout the near-surface region, indicating the level of agreement between the LES nondimensional potential temperature gradients and the similarity profile of Businger et al. (1971). The heterogeneous cases all significantly overestimate the modeled surface heat flux at every level. The error increases with decreasing Z_m and is significantly larger for the 6 K temperature jump simulations than the 3 K ones. The error in the model estimates is directly related to the increased potential temperature gradients observed in Fig. 7b. The surface temperature heterogeneity results in decreased cooling in the boundary layer, creating a large difference between

Unauthenticated | Downloaded 11/08/25 05:53 PM UTC

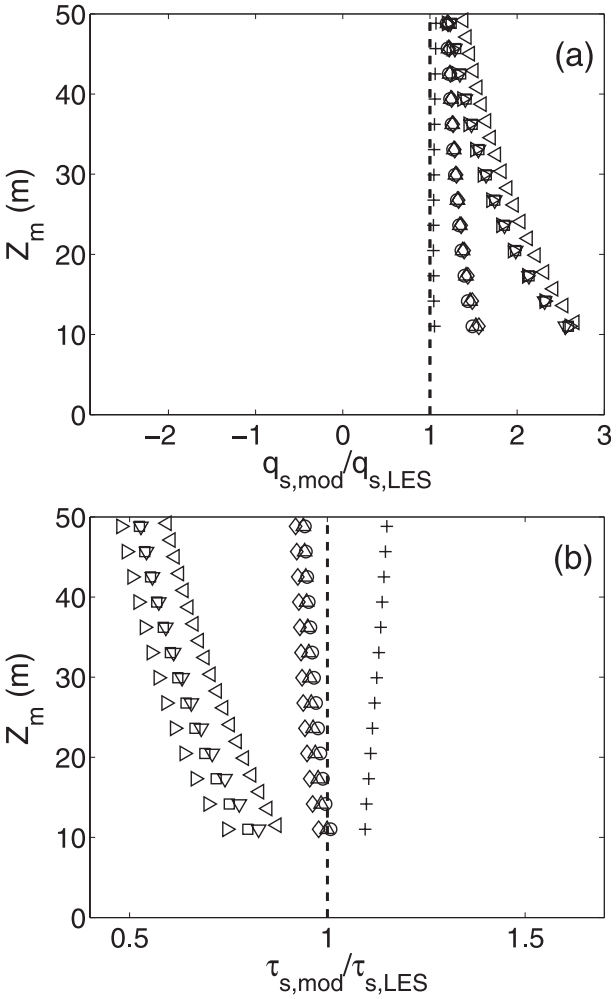

FIG. 10. Modeled value divided by LES value for (a) surface heat flux and (b) surface stress computed from the bulk parameterization method; Z_m is the height of the lowest computational level in a large-scale model and the graph symbols are as in Table 2.

the mean boundary layer potential temperature and the surface temperature. Bulk parameterizations relate this difference to the surface flux, with the effect of stratification only introduced through average stability corrections. No allowance is made for the contribution of advection of cold air over a relatively warmer surface, which can decrease the average heat flux. This has been recognized as a problem with bulk parameterizations in heterogeneous SBLs (Mahrt 1987; Claussen 1991; Blyth et al. 1993; Blyth 1995).

The bulk parameterization for the modeled surface shear stress ($\tau_{s,mod}$) results in predictions that are closer to the simulated stresses than the bulk model surface heat fluxes discussed previously. In Fig. 10b, the Het3 cases are all estimated within 20% at the tested heights when using Eq. (1). Given the 15% error for the homogeneous case, this can be considered reasonable. The Het6 cases result in larger deviations but still not on the order of the surface heat flux estimates. This agrees with Fig. 7a and further indicates that surface temperature heterogeneity has a minimal effect on the relationship between the mean velocity distribution and the surface stress. This small dependence on surface heterogeneity may be due to the relatively large geostrophic wind used in the simulations. Under weak wind conditions, with smaller average mean shear, buoyancy forces could have a more appreciable effect on the mean velocity field.

The tile model (Avissar and Pielke 1989; Claussen 1991; Ament and Simmer 2006) seeks to correct problems with the bulk parameterization approach by calculating the surface stress and heat flux locally over each different surface temperature patch. Figure 11 shows the surface heat flux and shear stress predictions using Eqs. (10) and (11) divided by the averaged LES values. For the surface heat flux in Fig. 11a, the tile model predicts the wrong sign for the average surface heat flux for the Het6 cases and the Het3 cases above the lowest tested level. Prediction of an unstable boundary layer is particularly problematic. Some insight into this poor performance can be gained by exploring heat flux estimates from the tile model over the individual patches. In Fig. 12, the ratio of the tile model prediction to the LES prediction for the surface heat flux over the two different surface types is shown. Both predictions have the correct sign for the heat flux, but although the prediction for the hotter (unstable) patch is roughly within 50% at most heights for all the cases, the flux prediction over the colder (stable) patch is much smaller and becomes completely insignificant above 20 m. Using randomly distributed bulk Richardson numbers with equations similar to (10) and (11), Mahrt (1987) showed that the nonlinearity of the stability correction given by Eqs. (12) and (13) can lead to unstable regions dominating grid-averaged surface flux calculations. For the cases studied here, the tile model reproduces this behavior and, combined with the inability of the linear stability corrections [Eqs. (6) and (7)] to produce reasonable fluxes over the stable regions, leads to the poor results shown in Fig. 11a.

The surface shear stress estimates in Fig. 11b have a departure from the LES values similar to that of the estimates with the bulk parameterization method for smaller Z_m values. The predictions for the Het6 cases show definite improvement over those in Fig. 10, especially as Z_m increases; but, compared to errors in the flux parameterizations, these improvements are insignificant. The strong mean shear masks variations in the buoyancy forces over individual patches, making the tile

Unauthenticated | Downloaded 11/08/25 05:53 PM UTC

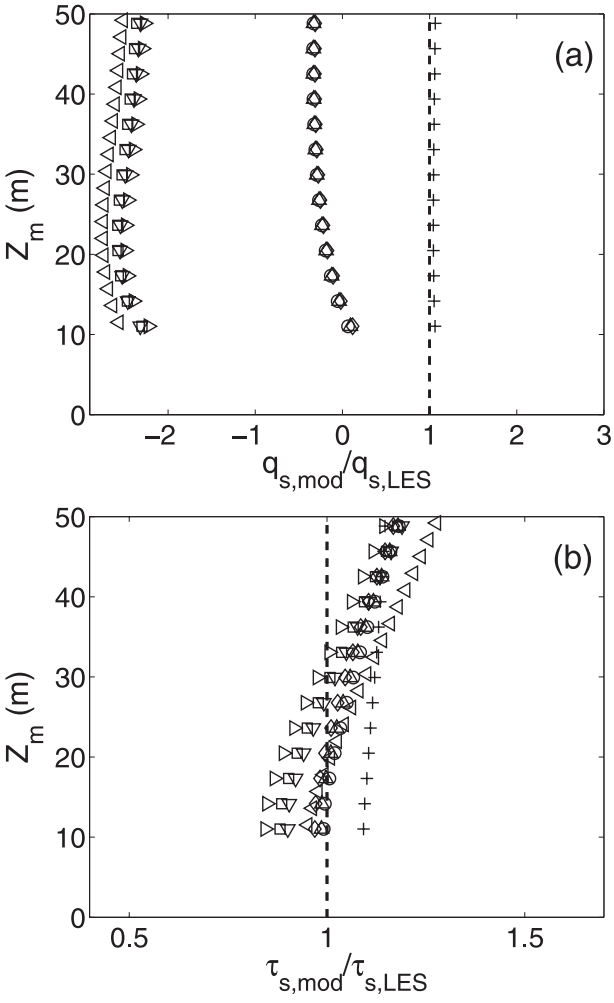

FIG. 11. As in Fig. 10, but computed from the tile model.

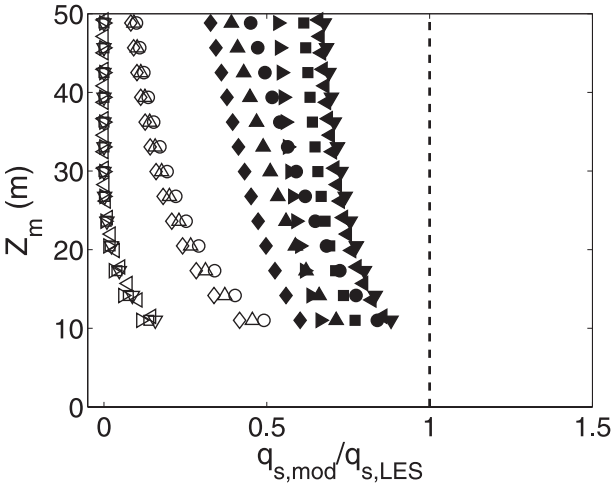

FIG. 12. Modeled value divided by LES value for surface heat flux over individual patches computed from the tile model; Z_m is the height of the lowest computational level in a large-scale model. Graph symbols are given in Table 2; open symbols correspond to cold patches and filled symbols to hot patches.

and bulk model shear stress formulations approximately equivalent.

The tile model attempts to include heterogeneity in a more explicit manner than bulk parameterizations by calculating fluxes and stresses over individual land cover types, but it does not address the effects of advection. In section 2, the extended tile model (Blyth et al. 1993; Blyth 1995; Arola 1999) was introduced as a way to account for advection in the tile model. Figure 13 compares predictions from this method to the LES surface fluxes. Here, the blending height of Mason (1988) is adopted. In Fig. 13b the surface shear stress predictions for all the surface temperature configurations fall within a range similar to that of the original tile model, with slightly worse results for the Het6 cases at the largest Z_m values. The inclusion of a blending height has a more pronounced effect on the prediction of the surface heat flux shown in Fig. 13a. For the simulations with weak advection effects (the Het3 cases), the extended tile model significantly improves the average flux predictions with respect to the basic tile model. In these cases the model predicts the correct sign for the average surface heat flux and, for the 100- and 200-m patch cases, reasonable magnitude estimates (within 50%). The same is not true for the Het6 cases. The extended tile model predicts the incorrect sign for all the Het6 cases at almost all heights. The only exception is a few of the uppermost levels for the Het6–100 case. This is a result of a large underprediction of the surface heat flux over the individual cold patches (40%–60% of the LES surface flux for the cold patches), similar to that discussed above and depicted in Fig. 12 for the tile model.

c. *Modified parameterization for heterogeneous SBLs*

In section 4b, existing parameterizations for the average surface stress and heat flux in large-scale models were tested using the LES dataset. None of the tested models properly reproduced the average surface heat flux. This is attributed to a failure to properly represent the heat flux over the colder patches. Over the warm patches, standard Monin–Obukhov similarity relations worked adequately when applied at the blending height. Because of this, the focus of this section is on improving the surface heat flux estimates over the colder (stable) patches. To accomplish this, modifications to the extended tile method are proposed. These modifications draw on the strengths of the tile model and blending

Unauthenticated | Downloaded 11/08/25 05:53 PM UTC

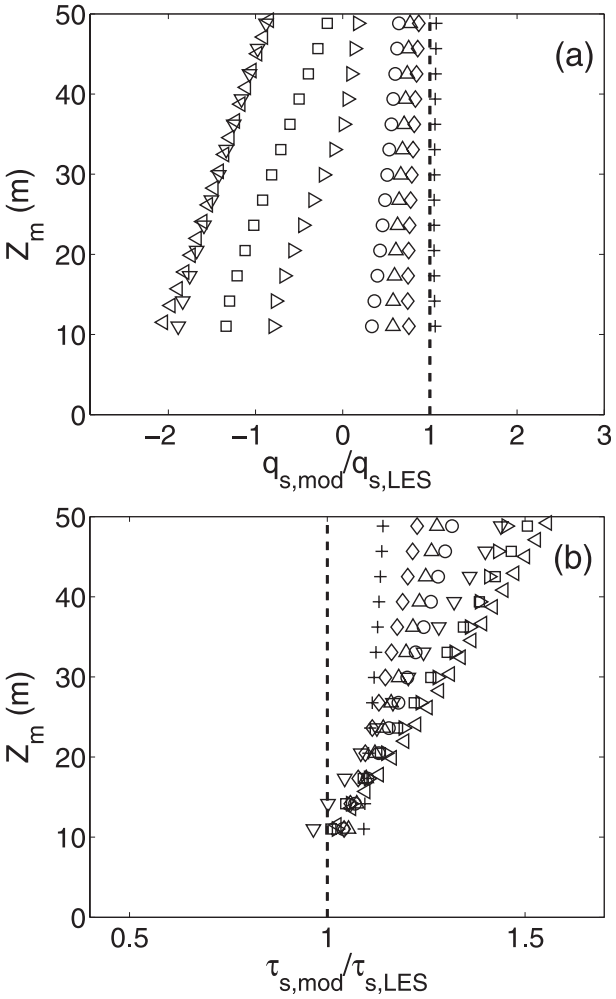

FIG. 13. As in Fig. 10, but computed from the extended tile method.

height concepts and combine them with ideas from Nieuwstadt's local scaling hypothesis (Nieuwstadt 1984, 1985).

1) NEW MODEL FORMULATION

Local scaling was introduced in section 4a. Figure 9 demonstrated that the average heat flux and shear stress profiles from simulations over both homogeneous and heterogeneous surface temperature distributions support the local scaling hypothesis. Moreover, individual heat flux profiles over the cold patch have near-linear behavior in the surface layer (see Fig. 4a). In homogeneous SBLs, Delage (1997) proposed to use local scaling, combined with surface layer similarity relations, to calculate the average surface flux. Here, the same general methodology is used to formulate the surface fluxes over individual patches by assuming that the patch fluxes follow local scaling up to the blending height.

Over the stable patches, the local patch-averaged heat flux q_ℓ and the local patch-averaged friction velocity $u_{*,\ell}$ are both assumed to vary linearly from their surface values up to their values at the blending height l_b, following

$$q_\ell = q_{s,i}\left[\left(\frac{q_b}{q_{s,i}} - 1\right)\frac{z}{l_b} + 1\right] \quad \text{and} \tag{23}$$

$$u_{*,\ell} = u_{*,i}\left[\left(\frac{u_{*,b}}{u_{*,i}} - 1\right)\frac{z}{l_b} + 1\right], \tag{24}$$

where q_b is the heat flux at l_b, $u_{*,b}$ is the friction velocity at l_b, the subscript ℓ denotes a local (height dependent) variable, the subscript b is a value at l_b, and the subscript i is an individual patch-averaged value. The linear dependence of $u_{*,\ell}$ on height z differs from the original dependence derived by Nieuwstadt (1985). Nieuwstadt showed that $u_{*,\ell} \sim z^{3/4}$, based on the assumption of constant gradient and flux Richardson numbers. Delage (1997) employed a simplification similar to Eqs. (23) and (24) and showed that it provided an adequate approximation for the $z^{3/4}$ behavior while simplifying the derived stability corrections. Furthermore, for the case of surface temperature heterogeneity in the presence of strong mean shear, the deviations from the mean friction velocity in the surface layer are small (e.g., Fig. 5a) and therefore results for $l_b \ll H$ should be insensitive to the details of Eq. (24).

The nondimensional wind speed and potential temperature gradients over the stable patches can be expressed using local stresses and fluxes as

$$\frac{\partial M}{\partial z}\frac{\kappa z}{u_{*,\ell}} = \Phi_M\left(\frac{z}{\Lambda}\right) \quad \text{and} \tag{25}$$

$$\frac{\partial \theta}{\partial z}\frac{\kappa z}{\theta_{*,\ell}} = \Phi_H\left(\frac{z}{\Lambda}\right), \tag{26}$$

where Λ is the local Obukhov length defined using $u_{*,\ell}$ and q_ℓ, and $\theta_{*,\ell} = -q_\ell u_{*,\ell}^{-1}$. Mahrt and Vickers (2003) term this type of formulation "hybrid similarity theory" because it asymptotically approaches surface layer similarity for small values of z and tends toward "z-less" scaling (Wyngaard 1973) for large z values.

Equations (25) and (26) can be combined with Eqs. (23) and (24) and then integrated from z_o to z to obtain a relationship describing the dependence of the wind speed and potential temperature at a given height on the patch-averaged surface heat flux and stress:

$$M(z) = \frac{u_{*,i}}{\kappa}\left[\ln\left(\frac{z}{z_o}\right) - \Psi_M\left(\frac{z}{L_i}, \frac{z}{l_b}, \frac{u_{*,b}}{u_{*,i}}, \frac{q_b}{q_{s,i}}\right)\right] \quad \text{and} \tag{27}$$

Unauthenticated | Downloaded 11/08/25 05:53 PM UTC

$$\theta(z) = \frac{\theta_{*,i}}{\kappa}\left[\alpha \ln\left(\frac{z}{z_o}\right) - \Psi_H\left(\frac{z}{L_i}, \frac{z}{l_b}, \frac{u_{*,b}}{u_{*,i}}, \frac{q_b}{q_{s,i}}\right)\right]. \quad (28)$$

The new stability correction functions Ψ_M and Ψ_H are defined by

$$\Psi_M\left(\frac{z}{L_i}, \frac{z}{l_b}, \frac{u_{*,b}}{u_{*,i}}, \frac{q_b}{q_{s,i}}\right) = \int_0^{z/L_i} \left[1 - \Phi_M(\zeta, A, B)(A\zeta + 1)\right] \frac{d\zeta}{\zeta} \quad \text{and} \quad (29)$$

$$\Psi_H\left(\frac{z}{L}, \frac{z}{l_b}, \frac{u_{*,b}}{u_*}, \frac{q_b}{q_s}\right) = \int_0^{z/L_i} \left[\alpha - \Phi_H(\zeta, A, B)\frac{(B\zeta+1)}{(A\zeta+1)}\right] \frac{d\zeta}{\zeta}, \quad (30)$$

where Eqs. (23) and (24) have been used to represent the dependence of the local Obukhov length Λ on z, and A and B are given by

$$A = \left(\frac{u_{*,b}}{u_{*,i}} - 1\right)\frac{L_i}{l_b} \quad \text{and} \quad B = \left(\frac{q_b}{q_{s,i}} - 1\right)\frac{L_i}{l_b}. \quad (31)$$

In Eqs. (29) and (30), the assumption that $z_o \ll L_i$ has been used to remove any dependence of the stability corrections on the aerodynamic roughness length.

Equations (29) and (30) require functional forms of $\Phi_M\left(zL_i^{-1}, A, B\right)$ and $\Phi_H\left(zL_i^{-1}, A, B\right)$. For stable conditions, Eqs. (19) and (20) can be used with the local stability parameter $z\Lambda^{-1}$ replacing zL_i^{-1} (Mahrt and Vickers 2003). With these similarity functions, integration of Eqs. (29) and (30) results in the following stability corrections for the patch wind speed and potential temperature profiles given by Eqs. (27) and (28):

$$\Psi_M = -A\zeta - \beta_M \times \left[\frac{B-A}{A^2(A\zeta+1)} - \frac{B-A}{A^2} + \frac{B}{A^2}\ln(A\zeta+1)\right] \quad \text{and} \quad (32)$$

$$\Psi_H = \alpha\frac{B-A}{B}\ln(A\zeta+1) + \beta_H\left[\frac{(3B^2\zeta^2 + 3B\zeta + 1)A^2 + (3B\zeta+1)BA + B^2}{3A^3(A\zeta+1)^3} - \frac{A^2 + BA + B^2}{3A^3}\right], \quad (33)$$

where $\zeta = zL_i^{-1}$ is the surface layer stability parameter for the patch.

Although Eqs. (32) and (33) appear complex, they are comprised of the same variables as other standard stability corrections [e.g., Eqs. (6) and (7)]. The exception to this is the need to specify the average heat flux and shear stress at the blending height. In section 4a (see Fig. 9), the average heat flux and shear stress vertical profiles from all of the heterogeneous cases were shown to follow the trend predicted by Nieuwstadt (1984, 1985). Using this and Delage's (1997) approximation for the stable surface layer, $\langle u_{*,\ell}\rangle$ and $\langle q_\ell\rangle$ are specified to have linear profiles defined by

$$\langle q_\ell\rangle = \langle q_s\rangle\left(1 - \frac{z}{H}\right) \quad \text{and} \quad (34)$$

$$\langle u_{*,\ell}\rangle = \langle u_*\rangle\left(1 - \frac{z}{H}\right). \quad (35)$$

The heat flux and stress at the blending height are found by evaluating these equations at $z = l_b$. Provided that l_b is significantly smaller than H, only a rough estimate of the boundary layer height is required and a relatively simple formulation can be employed (e.g., Zilitinkevich 1972).

The procedure to calculate the average surface heat flux and stress using these new stability corrections closely follows the extended tile model described in section 2. In addition to stability corrections for the individual stable patches, stability corrections are needed to extrapolate the mean wind speed and potential temperature from Z_m to l_b when using Eqs. (15) and (16). Here, instead of assuming constant mean fluxes up to the model height, Eqs. (34) and (35) are used with local similarity relationships for the mean wind speed and potential temperature analogous to Eqs. (25) and (26) to define mean field stability corrections:

$$\Psi_M = \frac{z}{H} + \beta_M\frac{H}{L}\ln\left(\frac{H-z}{H}\right) \quad \text{and} \quad (36)$$

$$\Psi_H = -\beta_H\frac{z}{L}\frac{H}{H-z}. \quad (37)$$

These stability corrections are nonlinear forms of those given by Eqs. (6) and (7), and for $z \ll H$ they have the same behavior. The main effect of Eqs. (36) and (37), in comparison to Eqs. (6) and (7), is to reduce the mean surface stress and heat flux for a given temperature difference between the surface and the air. Even though Eqs. (36) and (37) are undefined at $z = H$, it is envisioned that they will only be used in the near-surface region. Delage (1997) demonstrated the improvements of similar relationships in predicting surface fluxes of momentum and heat in homogeneous SBLs.

A few observations about the general behavior of the new stability corrections given by Eqs. (32) and (33) can

Unauthenticated | Downloaded 11/08/25 05:53 PM UTC

be made. First, both Ψ_M and Ψ_H will reduce to the mean stability corrections given by Eqs. (36) and (37), respectively, if $A = B = -LH^{-1}$ (i.e., in the homogeneous case). Second, both Eqs. (32) and (33) will result in increased stress and heat flux, respectively, for a given surface heat flux or stress contrast between the patches. In LES simulations of hot-to-cold and cold-to-hot sea surface temperature (SST) transitions, Skyllingstad et al. (2007) speculate that surface heat flux models for small-scale SST transitions should relate SST variance to the heat flux. Average profiles of surface temperature and buoyancy flux presented in section 4a lead to a similar conclusion here, and the behavior of Eqs. (32) and (33) described above encompasses this. Additionally, in section 4b it was demonstrated that existing models underestimate the surface heat flux over stable patches. The use of Eq. (33) is expected to improve upon this.

2) Evaluation of the new heterogeneous surface flux model

To test the new heterogeneous surface flux stability corrections, the LES dataset described in section 4a and used to test existing heterogeneous surface flux models in section 4b is used here. Figure 14 shows average surface flux estimates using the new stability corrections. The boundary layer height H required in the new stability corrections is taken from Table 2 and Mason's (1988) blending height [Eq. (14)] has been adopted. Tests using H from Zilitinkevich (1972) give similar results. For the surface shear stress predictions, results remain within the same range of values reported in section 4b for the other models. As discussed in section 4b, it is expected that momentum flux predictions would not be sensitive to the aggregation method. The new stability corrections have a much more pronounced effect on the surface heat flux predictions. The mean surface heat flux calculated using the extended tile model with the new patch and mean stability corrections shows a marked improvement over all of the other models. In contrast to the tile model and the extended tile model using traditional stability corrections, the new model predicts the correct sign of the average surface heat flux for all the cases. Not only does the model predict the correct sign, it also improves the magnitude of the heat flux prediction. This is a result of the enhanced negative heat flux created by the new stability corrections over the stable patches.

Figure 15 shows the heat flux over the individual patches. The new stability corrections have broken the trend seen in Fig. 12, where the heat flux over the stable patches is always underestimated to a greater degree than that over the unstable patches. In Fig. 15, a clear trend no longer exists between the different patch predictions. With the new stability corrections, as the surface

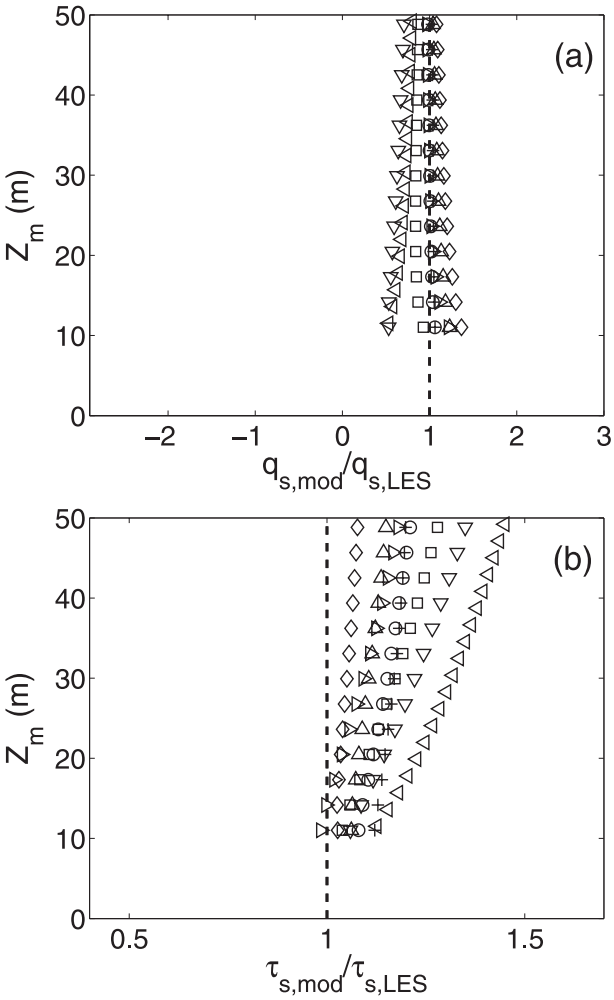

FIG. 14. Modeled value divided by LES value for (a) surface heat flux and (b) surface stress computed from the extended tile method with the new SBL stability corrections given by Eqs. (32) and (33); Z_m is the height of the lowest computational level in a large-scale model and the graph symbols are given in Table 2.

temperature patch contrast increases, the heat flux from the stable patch is enhanced. The standard linear stability corrections have the opposite effect. If the surface temperature contrast increases, the heat flux over the patch will decrease. The same is true as z increases. In the SBL, by definition, the potential temperature increases with increasing height. With standard stability corrections, increasing z results in decreased heat flux estimates. This gives some insight into why the tile model and extended tile model predictions degrade at larger Z_m values and for larger blending heights (i.e., larger patch sizes). The new stability corrections address both of these problems through the height-dependent patch flux profiles [Eqs. (23) and (24)] and the adjustment of the flux profile's slope based on the difference between the surface flux

Unauthenticated | Downloaded 11/08/25 05:53 PM UTC

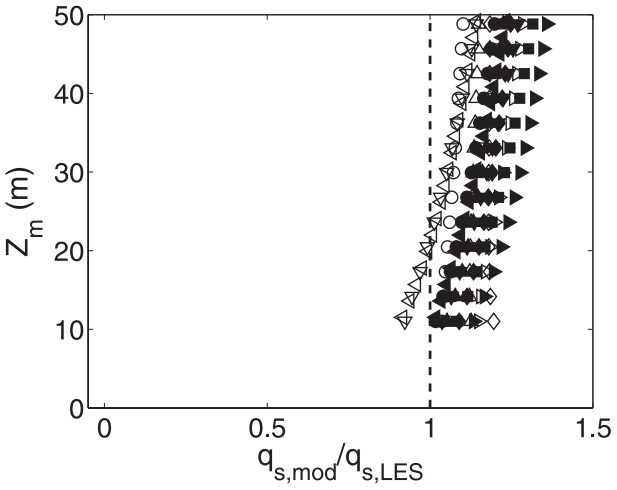

FIG. 15. Modeled value divided by LES value for surface heat flux over individual patches computed using the new SBL stability functions given by Eqs. (32) and (33); Z_m is the height of the lowest computational level in a large-scale model. Graph symbols are given in Table 2; open symbols correspond to cold patches and filled symbols to hot patches.

over the different patches. The net result is that the new corrections have the logical behavior expected for the case of warm air advected over a colder surface in a continuously turbulent SBL. The surface heat flux over the cold patch is enhanced by the increased difference between the local air temperature and the surface temperature.

5. Summary

Most natural land surfaces are heterogeneous over a wide range of spatial scales. Therefore, the modeling of average surface fluxes over heterogeneous terrain is of practical importance in mesoscale weather and climate models, which must specify these fluxes as surface boundary conditions. This study focuses on the particular case of parameterizations for the average surface shear stress and heat flux in stable boundary layers over heterogeneous surface temperature distributions. These parameterizations are explored using the large-eddy simulation technique.

A series of simulations over abrupt streamwise transitions in surface temperature are performed. The simulations are based on the homogeneous SBL case used in the intercomparison study of Beare et al. (2006). Two different temperature contrasts are tested (6 and 3 K) with three different patch length scales (100, 200, and 400 m) for each of the patch temperature differences. The simulation results reveal that for the cases studied here, the temperature contrast has a more pronounced effect on boundary layer statistics than the size of the patches. In particular, increasing the temperature contrast between the patches leads to increased boundary layer heights, elevated nocturnal jet formation, decreased average surface fluxes, and larger nondimensional potential temperature gradients in the near-surface region. The increased nondimensional potential temperature gradients preclude the use of standard Monin–Obukhov similarity theory to relate the average surface heat flux and the average potential temperature at the first level of a large-scale model. Despite these effects, the momentum flux and near-surface wind speed profiles are found to have relatively small sensitivity to the heterogeneous surface temperature distributions.

The set of simulations is also used to explore the performance of existing average surface flux model formulations. Three different formulations are examined: the bulk parameterization method (Mahrt 1996; Brutsaert 1998), the tile method (Avissar and Pielke 1989), and the extended tile method (Blyth et al. 1993; Blyth 1995). The bulk parameterization method is found to systematically overestimate the surface heat flux for all of the tested heterogeneous cases. The tile model and extended tile model both grossly underestimate the magnitude of the heat flux over the colder patches. For the cases with the largest advection effects, this leads to erroneous prediction of positive average heat fluxes. Motivated by these results a new model for the colder (stable) patches is developed. The new model combines ideas from local scaling (Nieuwstadt 1984, 1985) with the extended tile model. The model is presented as a set of new stability corrections to be used over the stable patches in conjunction with traditional stability corrections developed for the unstable ABL (Paulson 1970) over the hotter (unstable) patches both within the framework of the extended tile model. The new model is found to greatly improve the prediction of the average surface heat flux in all of the tested heterogeneous cases by allowing advection of warmer air over a colder surface to have more influence on the surface heat flux over the cold patches. The model does not require any new variables and can be implemented in weather and climate models as easily as the extended tile model.

Acknowledgments. The authors gratefully acknowledge funding from NSF (Grant EAR-0537856) and NASA (Grant NNG06GE256). R.S. was supported by a NASA Earth Systems Sciences fellowship (Training Grant NNG04GR23H). Computing resources were provided by the University of Minnesota Supercomputing Institute.

Unauthenticated | Downloaded 11/08/25 05:53 PM UTC

REFERENCES

Acevedo, O. C., and D. R. Fitzjarrald, 2001: The early evening surface-layer transition: Temporal and spatial variability. *J. Atmos. Sci.,* **58,** 2650–2667.

——, and ——, 2003: In the core of the night—Effects of intermittent mixing on a horizontally heterogeneous surface. *Bound.-Layer Meteor.,* **106,** 1–33.

Ament, F., and C. Simmer, 2006: Improved representation of land-surface heterogeneity in a non-hydrostatic numerical weather prediction model. *Bound.-Layer Meteor.,* **121,** 153–174, doi:10.1007/s10546-006-9066-4.

Arola, A., 1999: Parameterization of turbulent and mesoscale fluxes for heterogeneous surfaces. *J. Atmos. Sci.,* **56,** 584–598.

Avissar, R., and R. A. Pielke, 1989: A parameterization of heterogeneous land surfaces for atmospheric numerical models and its impact on regional meteorology. *Mon. Wea. Rev.,* **117,** 2113–2136.

——, and T. Schmidt, 1998: An evaluation of the scale at which ground-surface heat flux patchiness affects the convective boundary layer using large-eddy simulations. *J. Atmos. Sci.,* **55,** 2666–2689.

Beare, R. J., and M. K. MacVean, 2004: Resolution sensitivity and scaling of large-eddy simulations of the stable boundary layer. *Bound.-Layer Meteor.,* **112,** 257–281.

——, and Coauthors, 2006: An intercomparison of large-eddy simulations of the stable boundary layer. *Bound.-Layer Meteor.,* **118,** 247–272, doi:10.1007/s10546-004-2820-6.

Beljaars, A. C. M., and A. A. M. Holtslag, 1991: Flux parameterization over land surfaces for atmospheric models. *J. Appl. Meteor.,* **30,** 327–341.

Blyth, E. M., 1995: Using a simple SVAT scheme to describe the effect of scale on aggregation. *Bound.-Layer Meteor.,* **72,** 267–285.

——, A. J. Dolman, and N. Wood, 1993: Effective resistance to sensible- and latent-heat flux in heterogeneous terrain. *Quart. J. Roy. Meteor. Soc.,* **119,** 423–442.

Bou-Zeid, E., C. Meneveau, and M. B. Parlange, 2004: Large-eddy simulation of neutral atmospheric boundary layer flow over heterogeneous surfaces: Blending height and effective surface roughness. *Water Resour. Res.,* **40,** W02505, doi:10.1029/2003WR002475.

Brutsaert, W. H., 1998: Land-surface water vapor and sensible heat flux: Spatial variability, homogeneity, and measurement scales. *Water Resour. Res.,* **34,** 2433–2442.

Businger, J. A., J. C. Wyngaard, Y. Izumi, and E. F. Bradley, 1971: Flux-profile relationships in the atmospheric surface layer. *J. Atmos. Sci.,* **28,** 181–189.

Cassano, J. J., and T. R. Parish, 2001: Evaluation of turbulent surface flux parameterizations for the stable surface layer over Halley, Antarctica. *Mon. Wea. Rev.,* **129,** 26–46.

Chehbouni, A., and Coauthors, 2000: Methods to aggregate turbulent fluxes over heterogeneous surfaces: Applications to SALSA data set in Mexico. *Agric. For. Meteor.,* **105,** 133–144.

Claussen, M., 1990: Area-averaging of surface fluxes in a neutrally stratified, horizontally inhomogeneous atmospheric boundary layer. *Atmos. Environ.,* **24A,** 1349–1360.

——, 1991: Estimation of areally averaged surface fluxes. *Bound.-Layer Meteor.,* **54,** 387–410.

Cuxart, J., and Coauthors, 2006: Single-column model intercomparison for a stably stratified atmospheric boundary layer. *Bound.-Layer Meteor.,* **118,** 273–303, doi:10.1007/s10546-005-3780-1.

Delage, Y., 1997: Parameterising sub-grid scale vertical transport in atmospheric models under statically stable conditions. *Bound.-Layer Meteor.,* **82,** 23–48.

Derbyshire, S. H., 1995: Stable boundary layers: Observations, models and variability. Part I: Modelling and measurements. *Bound.-Layer Meteor.,* **74,** 19–54.

——, 1999: Stable boundary-layer modelling: Established approaches and beyond. *Bound.-Layer Meteor.,* **90,** 423–446.

Dyer, A. J., and E. F. Bradley, 1982: An alternative analysis of flux-gradient relationships at the 1976 ITCE. *Bound.-Layer Meteor.,* **22,** 3–19.

Högström, U., 1996: Review of some basic characteristics of the atmospheric surface layer. *Bound.-Layer Meteor.,* **78,** 215–246.

Holtslag, B., 2006: GEWEX atmospheric boundary-layer study (GABLS) on stable boundary layers. *Bound.-Layer Meteor.,* **118,** 243–246, doi:10.1007/s10546-005-9008-6.

King, J. C., W. M. Connolley, and S. H. Derbyshire, 2001: Sensitivity of modelled Antarctic climate to surface and boundary-layer flux parametrizations. *Quart. J. Roy. Meteor. Soc.,* **127,** 779–794.

——, A. Jrrar, and W. M. Connolley, 2007: Sensitivity of modelled atmospheric circulation to the representation of stable boundary layer processes. *Geophys. Res. Lett.,* **34,** L06708, doi:10.1029/2006GL028563.

Kondo, J., O. Kanechika, and N. Yasuda, 1978: Heat and momentum transfers under strong stability in the atmospheric surface layer. *J. Atmos. Sci.,* **35,** 1012–1021.

Kosović, B., and J. A. Curry, 2000: A large eddy simulation study of a quasi-steady, stably stratified atmospheric boundary layer. *J. Atmos. Sci.,* **57,** 1052–1068.

Louis, J.-F., 1979: A parametric model of vertical eddy fluxes in the atmosphere. *Bound.-Layer Meteor.,* **17,** 187–202.

Lüpkes, C., and G. Birnbaum, 2005: Surface drag in the Arctic marginal sea-ice zone: A comparison of different parameterisation concepts. *Bound.-Layer Meteor.,* **117,** 179–211, doi:10.1007/s10546-005-1445-8.

Mahrt, L., 1987: Grid-averaged surface fluxes. *Mon. Wea. Rev.,* **115,** 1550–1560.

——, 1996: The bulk aerodynamic formulation over heterogeneous surfaces. *Bound.-Layer Meteor.,* **78,** 87–119.

——, 1998: Stratified atmospheric boundary layers and breakdown of models. *Theor. Comput. Fluid Dyn.,* **11,** 263–279.

——, 2000: Surface heterogeneity and vertical structure of the boundary layer. *Bound.-Layer Meteor.,* **96,** 33–62.

——, and D. Vickers, 2002: Contrasting vertical structures of nocturnal boundary layers. *Bound.-Layer Meteor.,* **105,** 351–363.

——, and ——, 2003: Formulation of turbulent fluxes in the stable boundary layer. *J. Atmos. Sci.,* **60,** 2538–2548.

——, and ——, 2005: Boundary-layer adjustment over small-scale changes of surface heat flux. *Bound.-Layer Meteor.,* **116,** 313–330, doi:10.1007/s10546-004-1669-z.

——, J. I. MacPherson, and R. Desjardins, 1994: Observations of fluxes over heterogeneous surfaces. *Bound.-Layer Meteor.,* **67,** 345–367.

——, D. Vickers, and E. Moore, 2004: Flow adjustments across sea-surface temperature changes. *Bound.-Layer Meteor.,* **111,** 553–564.

Mason, P. J., 1988: The formation of areally averaged roughness lengths. *Quart. J. Roy. Meteor. Soc.,* **114,** 399–420.

——, and N. S. Callen, 1986: On the magnitude of the subgrid-scale eddy coefficient in large-eddy simulations of turbulent channel flow. *J. Fluid Mech.,* **162,** 439–462.

Unauthenticated | Downloaded 11/08/25 05:53 PM UTC

McCabe, A., and A. R. Brown, 2007: The role of surface heterogeneity in modelling the stable boundary layer. *Bound.-Layer Meteor.,* **122,** 517–534, doi:10.1007/s10546-006-9119-8.

Moeng, C.-H., 1984: A large eddy simulation model for the study of planetary boundary layer turbulence. *J. Atmos. Sci.,* **41,** 2052–2062.

Nieuwstadt, F. T. M., 1984: The turbulent structure of the stable, nocturnal boundary layer. *J. Atmos. Sci.,* **41,** 2202–2216.

——, 1985: A model for the stationary, stable boundary layer. *Turbulence and Diffusion in Stable Environments,* J. C. R. Hunt, Ed., Oxford University Press, 149–179.

Patton, E. G., P. P. Sullivan, and C.-H. Moeng, 2005: The influence of idealized heterogeneity on wet and dry planetary boundary layers coupled to the land surface. *J. Atmos. Sci.,* **62,** 2078–2097.

Paulson, C. A., 1970: The mathematical representation of wind speed and temperature in the unstable atmospheric surface layer. *J. Appl. Meteor.,* **9,** 857–861.

Porté-Agel, F., 2004: A scale-dependent dynamic model for scalar transport in large-eddy simulations of the atmospheric boundary layer. *Bound.-Layer Meteor.,* **112,** 81–105.

——, C. Meneveau, and M. B. Parlange, 2000: A scale-dependent dynamic model for large-eddy simulation: Application to a neutral atmospheric boundary layer. *J. Fluid Mech.,* **415,** 261–284.

Roy, S. B., and R. Avissar, 2000: Scales of response of the convective boundary layer to land-surface heterogeneity. *Geophys. Res. Lett.,* **27,** 4533–4536.

Saiki, E. M., C.-H. Moeng, and P. P. Sullivan, 2000: Large-eddy simulation of the stably stratified planetary boundary layer. *Bound.-Layer Meteor.,* **95,** 1–30.

Skyllingstad, E. D., R. M. Samelson, L. Mahrt, and P. Barbour, 2005: A numerical modeling study of warm offshore flow over cool water. *Mon. Wea. Rev.,* **133,** 345–361.

——, D. Vickers, L. Mahrt, and R. Samelson, 2007: Effects of mesoscale sea-surface temperature fronts on the marine atmospheric boundary layer. *Bound.-Layer Meteor.,* **123,** 219–237, doi:10.1007/s10546-006-9127-8.

Smagorinsky, J., 1963: General circulation experiments with the primitive equations. Part I: The basic experiment. *Mon. Wea. Rev.,* **91,** 99–164.

Smedman, A.-S., H. Bergstroöm, and B. Grisogono, 1997: Evolution of stable internal boundary layers over a cold sea. *J. Geophys. Res.,* **102,** 1091–1099.

Stoll, R., and F. Porté-Agel, 2006a: Dynamic subgrid-scale models for momentum and scalar fluxes in large-eddy simulations of neutrally stratified atmospheric boundary layers over heterogeneous terrain. *Water Resour. Res.,* **42,** W01409, doi:10.1029/2005WR003989.

——, and ——, 2006b: Effect of roughness on surface boundary conditions for large-eddy simulation. *Bound.-Layer Meteor.,* **118,** 169–187, doi:10.1007/s10546-005-4735-2.

——, and ——, 2008: Large-eddy simulation of the stable atmospheric boundary layer using dynamic models with different averaging schemes. *Bound.-Layer Meteor.,* **126,** 1–28, doi:10.1007/s10546-007-9207-4.

Taylor, P. A., 1987: Comments and further analysis on effective roughness lengths for use in numerical three-dimensional models. *Bound.-Layer Meteor.,* **39,** 403–418.

Tjernström, M., and Coauthors, 2005: Modelling the Arctic boundary layer: An evaluation of six ARCMIP regional-scale models using data from the SHEBA project. *Bound.-Layer Meteor.,* **117,** 337–381, doi:10.1007/s10546-004-7954-z.

Vihma, T., 1995: Subgrid parameterization of surface heat and momentum fluxes over polar oceans. *J. Geophys. Res.,* **100,** 22 625–22 646.

Viterbo, P., A. Beljaars, J.-F. Mahfouf, and J. A. Teixeira, 1999: The representation of soil moisture freezing and its impact on the stable boundary layer. *Quart. J. Roy. Meteor. Soc.,* **125,** 2401–2426.

Webb, E. K., 1970: Profile relationships: The log-linear range and extension to strong stability. *Quart. J. Roy. Meteor. Soc.,* **96,** 67–90.

Wieringa, J., 1986: Roughness-dependent geographical interpolation of surface wind speed averages. *Quart. J. Roy. Meteor. Soc.,* **112,** 867–889.

Wood, N., and P. Mason, 1991: The influence of static stability on the effective roughness lengths for momentum and heat transfer. *Quart. J. Roy. Meteor. Soc.,* **117,** 1025–1056.

Wyngaard, J. C., 1973: On surface-layer turbulence. *Workshop on Micrometeorology,* D. A. Haugen, Ed., Amer. Meteor. Soc., 101–149.

Zilitinkevich, S. S., 1972: On the determination of the height of the Ekman boundary layer. *Bound.-Layer Meteor.,* **3,** 141–145.

Unauthenticated | Downloaded 11/08/25 05:53 PM UTC